Assessment of time effects on capacities of large-scale piles driven in dense sands

Wen, K.[1], Kontoe, S. [1], Jardine, R.J. [1], Liu, T. [1], Cathie, D.[2], Silvano, R. [2], Prearo C.[2], Wei, S. [3], Schroeder, F.C. [4], Po, Stanislas [5]

1. Department of Civil & Environmental Engineering, Imperial College London, UK; 2. Cathie Associates, Diegem, Belgium; 3. Surbana Jurong Private Limited, Singapore; 4. Geotechnical Consulting Group LLP, London, UK; 5. Fugro, France.

ABSTRACT

This paper considers the axial resistances of open-ended, highly instrumented, 763 mm diameter steel pipe piles driven in sands for the EURIPIDES (EURopean Initiative on PIles in DEnse Sands) project at a well characterised research site at Eemshaven, in the northern Netherlands. It offers new analyses of previously unreported dynamic tests and considers their relationship to four heavily instrumented static compression tests. Rigorous signal matching employing two distinct pile-soil interaction models is reported, supported by careful sensitivity analyses, to interpret the recorded driving signals. The back-calculated shaft resistance profiles show good agreement between the models as well as calculations performed with a global wave equation analysis approach. The study highlights the need to account for the internal soil column resistance. The combined interpretation of the dynamic and static test data indicates a 50% gain in shaft resistance over the ten days after driving and threefold shaft capacity growth over a total period of 533 days after driving. The outcomes have important implications for driven pile design and field quality monitoring; the case history contributes an important benchmark in the study of long-term set-up trends.

Keywords: Time effects, pile capacity, sands, signal matching, large-scale static tests

INTRODUCTION

The EURIPIDES joint industry project (JIP) comprised instrumented dynamic, static (tension and compression) tests on 763 mm diameter open-ended steel piles driven in dense sands at a well-characterised harbour site in the Netherlands (Zuidberg and Vergobbi, 1996). The high-quality static tests aided the checking and development of CPT-based pile capacity assessment methods for sands, including the ICP-05 (Jardine et al. 2005), UWA-05 (Lehane et al. 2005) and Unified-20 (Lehane et al. 2020) approaches. However, the dynamic driving data has not yet been interpreted and integrated with the monotonic tests, including a compression re-test on an aged pile that has received relatively little prior attention. This paper presents new analyses of these missing elements and adds additional insights into the impact of field ageing on compression capacity, adding to earlier studies which focussed on tension testing; see Jardine et al (2006), Gavin et al. (2013) and Rimoy et al. (2015).

Dynamic pile testing involves monitoring pile responses to hammer blows that have sufficient energy to fully overcome the local soil resistances acting along the pile shaft and base as the compressive wave generated at the pile head travels downwards towards the tip and is partly reflected upwards due to interaction with the soil. Strains and accelerations measured near the pile top fed into one-dimensional stress wave analyses provide estimates of the static resistance to driving (SRD). Signal matching techniques utilize characteristic solutions of the wave equation and can model pile driving accurately without the need to model the hammer and cushion (Rausche et al. 1972; Middendorp and van Weel, 1986; Randolph 2008). The key input parameters include pile dimensions, soil properties that are required in the adopted pile-soil interaction models, and the distribution of soil resistance over depth that is adjusted iteratively until a good quality match is obtained between the measured and computed pile forces, F, or the product of velocity and pile impedance, Z , where pile impedance $Z = \sqrt{E\rho}A$, where E is Young's modulus, ρ is mass density and A is cross-sectional area. Aiming to improve these classical approaches, Salgado et al. (2015) divided the soil around the pile shaft into a series of thin horizontal discs and considered the motion phase differences developed along the pile and soil layers with different properties. Their developed shaft and base soil reaction models took soil non-linearity and hysteresis explicitly into account, with input parameters that have physical meaning and are linked to standard soil properties. However, signal matching cannot provide unique solutions and the pile 'capacities' obtained can depend on the operator and adopted pile-soil interaction model (see Fellenius 1988; Salgado et al. 2015; Buckley 2018). Signal matching was performed for the present study by two independent experts, each using different signal matching software; the commonly used CAPWAP (CAPWAP manual, 2006) package, and the research orientated code IMPACT (Randolph 2008) to address model uncertainty. While the analysts had access to the same information, they performed their analyses independently and only compared outputs from the final iterations of each of their analyses.

The influence on signal matching analyses of the internal soil column (ISC) formed when driving large pipe piles has not been investigated extensively in the literature. Most signal matching studies combine internal and external friction and treat end-bearing resistance as acting on the piles' annular bases. Randolph (1987) considered the ISC explicitly, treating it as a separate 'pile within a pile' and allowed axial compression wave propagation within the ISC. Brucy et al. (1991) argued that internal and external shaft resistances cannot be separated, illustrating this through their study of the ISC's influence on experimental pile driving in sand at Dunkirk, Northern France. They considered signals from blows applied to an open pile with (i) its ISC in place and (ii) after its removal, finding a large reduction in dynamic shaft resistance. Subsequent studies have confirmed that driving simulations can be improved by taking the ISC into account (Matsumoto and Takei, 1991; Schneider and Harmon, 2010; Doherty et al., 2020). However, broad agreement has yet to be established regarding the best ISC modelling approach for signal matching.

This paper presents and interprets previously unpublished pile dynamic testing from the EURIPIDES project, integrating these with companion static compression tests to establish systematic links between dynamic and static resistances. Both the Continuum (Randolph 2008) and Smith methods (Smith 1960) are employed for signal matching; the influence of internal shaft resistance is also evaluated and discussed as is the impact of pile age after driving.

OVERVIEW OF TESTING PROGRAMME

Site investigation

Figure 1 shows the EURIPIDES pile location at Eemshaven harbour. Two piles were driven 18 m apart, with nearby sampled boreholes (BH), cone penetration tests (CPT) and other in-situ tests. CPT36 & BH 36 were located within 5 m of Location 1, while CPT41 & BH 41 were positioned within 5 m of Location 2. On average, the water table was around 2.0 m below ground level (bgl).

Figure 2 (a) shows the stratigraphy and recorded CPT traces. Fine sand fill and topsoil were found above fine sand to around 15 mbgl, with an average q_c around 5 MPa. Very dense fine sand with q_c between 50 and 85 MPa was encountered 25 m bgl, with the sand becoming medium-to-coarse below 44 m bgl. Analysis of grain size measurements on borehole samples indicates that the dense sand layer of greatest interest (from between 28 – 50 mbgl) has an average D_{50} of 0.14 mm.

The profile of soil behaviour type index I_c (Robertson and Wride, 1998) is plotted in Figure 2(b) from the Location 1 q_c profile. Alternating layers of soft clay and loose sandy silt were encountered from roughly 16 m to 21 m bgl at Location 1, with $3 < I_c < 3.5$, which were treated as clay in later analyses. A similar layer was also noted at Location 2, although without sleeve friction f_s data to derive the corresponding I_c profile. Relative density D_R profiles derived using the q_c-D_R correlation of Lunne and Christoffersen (1983) indicated D_R close to 100% below 30 m, covering the main EURIPIDES target stratum. Also plotted in Figure 2(b) is the G_{max} profile from seismic piezocone (SCPTu) tests at Location 1, which is assumed to apply equally to Location 2.

Laboratory testing on borehole samples included index tests, triaxial and direct shear tests (Zuidberg and Vergobbi, 1996). Ring shear interface tests were also performed with steel interfaces that had maximum surface roughness of 25 μm close to that of the test piles. The measured interface friction angles, δ', were broadly 27° for the sands below 44 mbgl, and 31° for the finer sands found 22-44 mbgl. Interface shear tests were not conducted for the soils above 22 mbgl, so δ'=29° was adopted, except for the 15 to 22 mbgl "clay layer", where the CPT-based UWA-13 method (Lehane et al, 2013) was used to predict static shaft capacity without needing to specify an interface friction angle.

Characteristics of test piles

Table 1 and Figure 3 outline the general arrangements of the 763 mm outside diameter (D) piles. The Location 1 pile had a 27 m long instrumented section and a 22 m long upper add-on section. Two force rings were forged into the add-on approximately 33 and 41 m above the toe, resulting in local wall thicknesses around 90 mm which affected wave propagation during driving. The Location 1 pile was extracted and trimmed after testing, reducing the instrumented and add-on lengths to 26.9 m and 21.6 m respectively. The tabulated wall thicknesses values do not account for the pile instruments and cable channels. All pile sections were made of E460N steel, with density of 7.86 Mg/m^3 and a minimum 450 MPa yield stress that exceeded the expected 275 MPa maximum driving stress. All sections were weighed individually, giving 'equivalent' mass densities, ρ, that accounted for the instrumentation.

Pile instrumentation

Two sets of dynamic PDA strain gauge and accelerometer sensors were mounted at distances around 1.0 m (or 1.3D) below the pile heads, as estimated through back-analyses of the driving signals. The 7.88 m long pile driving system employed an IHC S-90 hydraulic impact hammer, standard ram, and an anvil. These components weighed 4500 and 800 kg, respectively. An IHC system recorded blow counts and average kinetic energy continuously during driving, providing information that was critical to the 'Global Match' process which is discussed subsequently.

The internal soil column (ISC) was monitored during driving by a tape system (Fugro 1996) which recorded its height after each 0.25 m of penetration. Measurements were also made during static testing. Fourteen levels of axial strain gauges were mounted on the lower section of the test piles to measure the distribution of axial forces and derive static shaft resistances. These axial strains were positioned 0.5D, 1.0D, 2.0D, 4.0D, 6.0D and 8.0D above the pile toe and every 4.0D to the highest level at about 40D. More details describing the configuration, use and performance of other circumferential strain gauges, total stress and toe load cells are provided in Zuidberg and Vergobbi (1996).

Pile driving sequences and records

Figure 4 shows the driving sequences at the two locations. Driving to the final penetrations (46.95 m and 46.65 m for Locations 1 and 2 respectively) was interrupted by: (i) welding of the add-on sections after driving to around 25 mbgl, (ii) both short and long operational pauses. Driving at Location 1 halted after penetration to 30.45 m and 38.70 m, and static tests performed after 7 and 2 day pauses respectively. Static tests were also performed 12 days after the end-of-driving to 46.95 m, after which the pile was extracted. Surface roughness and instrument damage checks were made before the ISC was removed. A buried tree trunk, 60-65 cm diameter, was found between 21.6 to 22.2 m above the toe, that fully occupied the pile's interior area and affected the blow counts measured over this penetration range. The influence of the cored tree trunk on the subsequent pile loading tests remains open to conjecture.

The pile was re-driven at Location 2 with several short operational pauses, and a 7 day pause for add-on and instrumented section welding. Static testing was only undertaken after driving to the final depth and imposing a 6 day pause. A compression re-test was conducted after 533 days of in-situ ageing, which did not achieve full failure.

Figure 4 presents the recorded blow counts and transferred driving energy profiles. The pile driving at Location 2 applied a lower hammer drop height and lower ENTHRU energy resulting in higher blow counts over the upper 15 m than at Location 1. Blow counts increased steadily from 40-50 blows/0.25 m to 100-150 blows/0.25 m, as the piles penetrated through the very dense sand below 30 mbgl. Higher local blow count spikes were evident after pauses caused by both the impact of ageing and the low initial ENTHRU energy developed when driving re-started. The ENTHRU energies fell in the 65-75 kJ range as the tips penetrated the dense layers (30-48 mbgl) with hammer global efficiency (the ratio of the ENTHRU energy to the 90-kJ kinetic energy of the ram) around 80% (±5%). The latter measurements allowed the SRD profiles to be assessed by the 'Global Match' process described later.

Figure 4 also shows the ISC levels during driving, where the negative sign refers to the depth below ground surface. The two locations exhibit broadly similar trends over most of the profile, although different rates developed between 5 mblg and 20 mbgl tip depths that left final ISCs that rose 0.5 m above ground level at Location 1 while being depressed by 2.3 mbgl at Location 2. The Incremental Filling Ratios (IFR) were close to unity throughout driving, indicating almost continuous coring.

When selecting dynamic blows for EoD analyses, those recorded at penetration tip depths closest to the available static pile tests were generally considered the most representative. Dynamic data quality was also assessed by checking the coincidence of F and Zv records as waves travelled from the PDA instruments down to the ground level. In cases where complementary pairs of strain gauge/accelerometer measurements were available, the consistency between the two outputs was also considered in evaluating signal quality.

Figure 5 plots the F and ZV traces of the three selected blows, following Savitzky-Golay filtering to reduce the signal noise from the raw records. The quality of the traces appears to be good, with the maximum force $F_{\max}$ matching ZV as the stress waves propagated along the free pile stick-up. Also given in Figure 5 are the values of t_o and $t(F_{max})$, which denote the onset of impact and the time corresponding to $F_{\max}$. The dynamic blows records extended to nearly 40 milliseconds, around twice the period for the waves to travel to the pile tip and back ($2L/c \approx 18$ ms).

Table 2 briefly summarises the information of selected blows and corresponding static tests, which are also labelled in Figure 4. Altogether, four series of static compression (C) and tension (T) tests were carried out that can be compared with the three dynamic EoD cases, along with some reloading tests (R) (Kolk et al. 2005). Only first-time compression tests were considered here as prior tension and reloading are known to degrade compression capacity significantly (Galvis-Castro et al. 2019) and so lead to erroneous comparisons with EoD resistances. The static tests conducted at Location 1 after driving to 38.7 m depth were discounted due to their T-R-C-T sequence.

As shown in Table 2, further consideration had to be given to selecting a suitable blow (Loc1_BN10) to compare with the static compression test Loc1_CP1. In this case, no EoD signal data was available from driving to this test's tip depth. The Loc1_BN10 record employed for analysis came from the 10th dynamic blow applied after completing the Loc1_CP1 static testing. The driving blow count profile in Figure 4 indicates that any pile capacity enhancement that occurred over the 12-day ageing pause allowed between EoD and testing was eliminated over these first ten blows. The Loc1_BN10 signals were taken as the best available proxies for the Loc1_CP1 test's EoD conditions.

The penetrations levels achieved in two other blows (Loc1_BN3001 and Loc2_BN3315) are slightly shallower than for the corresponding static tests (see Table 2). This difference might lead to slight overestimates of shaft set-up factors in the subsequent analyses.

SIGNAL MATCHING METHODOLOGY

Signal matching was performed with the industry-standard CAPWAP software (CAPWAP manual, 2006) using Smith model and with the research-oriented IMPACT software developed by Randolph (2008) using a Continuum model. The rheological models' characteristics are set out in Table 3 and the main points are highlighted below.

Smith model

The Smith model (Smith 1960) comprises a dashpot, representing all soil damping effects, and a system of a linearly elastic spring and a plastic slider connected in series. The total shaft resistance (dynamic + static), τ, associated with both the local pile shaft displacement, $w_{p,s}$, and the pile shaft velocity, $v_{p,s}$, is expressed as:

$$\tau = Min\left(1, \frac{w_{p,s}}{Q_{p,s}}\right)\left(1 + J_s v_{p,s}\right)\tau_s \qquad \text{Eq. 1}$$

Where $Q_{p,s}$ is the so-called shaft 'quake' at which the limiting static shaft resistance, τ_s, is fully mobilised. If the $w_{p,s}$ exceeds $Q_{p,s}$, then the plastic slider is activated, and perfectly plastic deformation starts to develop. J_s is Smith's soil damping constant (in s/m) associated with the viscous dashpot. Smith's base model comprises of similar components, expressed mathematically by a similar formula to Eq. 1. The main difference between the shaft and base models is that, during the unloading stage, no tensile end bearing is allowed at the base, so the lower bound base resistance is zero. The Smith dashpot remains active regardless of the pile slip; viscous and inertial damping are lumped into a single dashpot that is proportional to τ_s. The quake and damping modelling constants determined empirically from back-analyses of pile driving records and pile load tests generally fall within a relatively narrow range. Rausche et al (2010) reports typical $Q_{p,s}$ ranges as 1–7.5 mm for sands and clays, with $Q_{p,b}$ in the range of 1.0mm to the maximum pile toe displacement, independent of pile diameter. Smith damping constants are generally taken in the range 0.1–0.2 s/m at the pile shaft node, and 0.1 s/m (sand) – 0.5 s/m (clay) at the pile base (Cho et al., 2000).

Although not employed in the present study, Likins et al. (1992) presented an extended Smith model using the soil mass and dashpots at the pile shaft and base to represent radiation damping. Their mass was a function of the pile perimeter and segment length, whereas the dashpot was given in terms of pile impedance. They suggested limiting the maximum damping factor to 1.3 s/m led to better correlations with static loading test resistances.

Continuum model

Simons and Randolph (1985) developed their Continuum model by introducing an additional degree of freedom, based on the closed-form solution by Novak et al. (1978) for the soil resistance acting along the shaft of a rigid infinitely long pile. The shaft model comprises a spring and radiation dashpot connected in parallel, followed by a system of a plastic slider and viscous dashpot set in series. Unlike the Smith model, the viscous dashpot simulates the shear band forming at the shaft after pile sliding, which is subjected to viscous rate effects, while inertial (radiation) far-field soil damping is represented by an inertial dashpot. The pile shaft response prior to slip is expressed as:

$$\tau = \frac{G}{D} w_{s,s} + \sqrt{G\rho_s} v_{s,s} \leq \tau_{lim} \qquad \text{Eq. 2}$$

Where G is the soil shear modulus; $w_{s,s}$ and $v_{s,s}$ are the soil displacement and velocity adjacent to the shaft respectively, and τ_{lim} is a velocity-dependent limiting resistance at pile-soil interface (see Eq. 3). If $\tau > \tau_{lim}$, slip at the pile-soil interface starts to occur and little further energy is propagated into the soil mass. At that moment, the interface response is then modelled by the plastic slider in parallel with the viscous dashpot. A power law function is employed to define τ_{lim}, which augments the static limiting shaft resistance τ_s as pile-to-soil relative velocity, Δv, grows (Coyle and Gibson, 1970)

$$\tau_{lim} = \tau_s \left[1 + \alpha \left(\frac{\Delta v}{v_{ref}}\right)^{\beta}\right] \qquad \text{Eq. 3}$$

Where v_{ref} is the reference velocity, taken as 1.0 m/s; α and β are viscosity parameters. Litkouthi and Poskitt (1980) suggest $0.2 < \beta < 0.5$. Randolph (2003) indicates α is 0.3 to 0.5 for sand, and up to 2 or 3 for clays.

The Continuum base model adopts a broadly analogous configuration, except for two lumped masses connecting to the pile node (m_0) and also through a second radiation dashpot (m_1) (Deeks and Randolph, 1995). For undrained conditions as appropriate for pile driving, it turned out the subsidiary mass (m_1)

is zero and hence its connected radiation dashpot is neglected. The spring and inertial dashpot parameters are determined from fundamental soil properties. The model formulation is expressed as:

$$\frac{2GD}{1-\nu}w_{s,b}+\frac{0.8D^2}{1-\nu}\sqrt{G\rho_s}v_{s,b}\leq q_bA \qquad \text{Eq. 4}$$

where $v_{s,b}$ and $w_{s,b}$ are the velocity and displacement of the soil beneath pile base; ν is Poisson's ratio; G is shear modulus of soil; and A is cross section area at pile base.

Simulation of internal soil column

Open-ended piles mobilise shaft resistance along their internal and external shaft areas and simulating the internal soil column (ISC) resistance improves back analysis of their driving records (Doherty et al., 2020). In CAPWAP and in similar commercially signal matching-based software, the internal soil resistance is not considered separately. Randolph (1987) modelled the ISC explicitly in his Continuum approach by treating the dynamic response of the soil inside the pile in a similar way to that outside the pile with lumped masses connected by a spring and a dashpot. Wave propagation through the ISC is assumed to be transferred as a shear wave emanating from the pile wall. Identical model components are employed for the ISC, except for minor changes in the displacement and velocity terms. The internal shaft shear force per unit length, $T_{s,in}$, is expressed as

$$T_{s,in}=5.5G\left(w_{sp1}-w_{sp2}\right)+\pi D\frac{G}{V_s}(v_{sp1}-v_{sp2}) \qquad \text{Eq. 5}$$

Where w_{sp1} and w_{sp2} are the displacement of soil nodes adjacent to the shaft area and at the centre of ISC respectively; v_{sp1} and v_{sp2} are the corresponding velocities; G is the shear modulus for ISC; V_s is the shear wave velocity.

Match quality assessment

Multiple objective matching approaches are proposed in the literature to evaluate the degree of agreement between the measured and computed signal traces through quality indices M_q whose precise formulations vary between Authors and codes. Middendorp (2015) and Buckley (2018) used an M_q formula that considered six specified intervals of the upward travelling wave and is suitable for dynamic signals with long time periods. However, recalling the relatively short EURIPIDES driving signal records (≤ 40 ms), an adjusted procedure was followed for the present IMPACT analyses:

(a) The signal was divided into four periods, as in Figure 6. t_r is the time from t_o to $t(F_{max})$.

(b) Match quality was assessed by considering both the force and ZV signals from upward (F_u) and downward (F_d) travelling waves, as indicated by Eq. 6.

$$F_u = \frac{F-ZV}{2} \qquad \text{Eq. 6a}$$

$$F_d = \frac{F+ZV}{2} \qquad \text{Eq. 6b}$$

(c) The absolute difference between the measured and computed upward forces ($F_{u,m}$ and $F_{u,c}$ respectively) were added at each time increment over each time interval and then normalised by F_{max} times the numbers of time increments, n_{sample}, in this time interval.

(d) The computed sum values for the four time periods from step (b) were then averaged to obtain the overall M_q by:

$$M_q = 0.25 \times \sum_{Period} \sum \frac{|F_{u,m} - F_{u,c}|}{n_{sample} \times F_{max}} \times 100 \qquad \text{Eq. 7}$$

Note that the procedure developed above to address the relatively short EURIPIDES signal durations does not consider the degree of matching w_p separately.

For CAPWAP analyses, the standard built-in match quality tool was employed, which divided the records into four time periods that do not coincide with the time intervals adopted for the IMPACT quality assessment described above (Rausche et al. 2010). The CAPWAP criterion includes a blow count penalty for w_p, which is calculated as the absolute value of the difference between the observed and calculated final set, minus 1 mm, as detailed by Rausche et al. (2010) and the CAPWAP manual (2006).

While the M_q values produced from IMPACT and CAPWAP are not directly comparable due to their different calculation strategy and units, lower M_q values signify better signal matching in both cases. It is recognised that specifying absolute and general M_q values as quality control parameters is impractical, even when using a single definition as each dynamic dataset has its own optimum (Rausche et al. 2010).

BACK ANALYSIS OF DYNAMIC PILE TESTS

It is well established that signal matching outcomes obtained with Smith's model vary with the primary input parameters (Liang and Sheng, 1993; Ng and Sritharan, 2013). However, the relative sensitivity of outcomes to the Continuum model parameters and assumptions is less clear. The parametric IMPACT study presented in Appendix A explores this potential sensitivity, focussing Loc 1_BN10 as an example hammer blow.

The sensitivity study highlights the influence of modelling the internal soil column (ISC) on signal matching. Employing the plug modelling facility built into IMPACT and considering a range of internal resistance assumptions indicated that the best quality signal matches were yielded when setting the internal local shaft resistance ($\tau_{s,in}$) equal to 10-20% $\tau_{s,out}$ (see Appendix A). Although constant ratios of inner-to-outer shaft resistance are usually assumed over the full plug length in dynamic pile testing (Alm and Hamre, 2001; Schneider and Harmon, 2010; Doherty et al., 2020), further theoretical and experimental research is required to explore the true distributions of local $\tau_{s,in}/\tau_{s,out}$ ratio.

Table 4 provides the main input parameters adopted for the Continuum and Smith modelling of the three blows after performing sensitivity studies. Viscosity parameters α for external shaft resistance ranged 0.25-0.45, while $\beta = 0.2$ was adopted in all cases. The ISC viscosity parameters were taken as equal to those applied externally. The Poisson's ratio, ν, was taken as 0.5 to represent the potentially undrained conditions applying beneath the pile tip over the short hammer blows.

The best fitted limiting bearing pressures beneath the pile annulus ($q_{\mathrm{b,a}}$) were 0.51-0.59q_c in the IMPACT analyses, while the CAPWAP analyses, $q_{\mathrm{b,a}}$ indicated a notably lower 0.12-0.35q_c range. While the true values are uncertain, these ratios are in keeping with ranges quoted by Alm and Hamre (2001), Schneider and Harmon (2010). The incremental pile displacements mobilised during dynamic testing are far less than the 0.1D displacement at which static base capacity is often defined and the dynamic $q_{\mathrm{b,a}}/q_{\mathrm{c}}$ ratios are lower than that may be mobilised in fully plunging pile failure for which far higher $q_{\mathrm{b,a}}/q_{\mathrm{c}}$ ratios apply, especially if the pile plugs (Jardine et al. 2005; Lehane et al. 2005; or Xu et al. 2008).

The piles were divided into six segments for the signal matching analyses, including two separate segments representing the force rings. Figure 7 shows the 'best possible matches' between the calculated and measured upward travelling force ($F_{u,c}$ and $F_{u,m}$ respectively) and displacement at pile head w_p. The Continuum model outputs match the measured data well throughout the three blows' loading histories, which is also quantitively evaluated by M_q values calculated as outlined above. The Smith model also gives good fits, except for Loc1_BN10 over the unloading phases (after t_o+ 2L/c), where an abrupt increase in w_p took place, probably due to the presence of thin alternating soft soil layer beneath pile tip. It seems that in these circumstances, simulating viscous and inertial damping separately produces better match to the measured signals.

Figure 8 compares the back-calculated Static Resistance to Driving (SRD) noted at three discrete pile tip depths with the full-depth driving predictions from the Alm and Hamre (2001) SRD method, as well as the ICP-05 and Unified-20 sand approaches for predicting static capacity after allowing moderate (14 to 25 day) ageing set-up periods. The UWA-13 clay procedures (Lehane et al. 2013) were applied to estimate pile resistances within the (16-21m bgl.) "clay-layer". As expected, the Alm and Hamre (2001) driving SRD profile falls well below that predicted by the two static capacity methods, which implicitly allow for set-up to occur before testing at 'medium-term' ages after driving.

Also plotted in Figure 8 is the 'Global Match' SRD profile obtained for this study by processing the pile driving records with the ALLWAVE-PDP approach (Allnamics, 2015), which uses one-dimensional wave equation theory combined with the Smith (1960) soil resistance model. The parameters fed into the 'Global Match' analyses are:

(1) The blow count records from each location (see Figure 4), excluding any blows applied after ageing and operational driving pauses;

(2) The hammer ram and anvil characteristics as well as the measured ENTHRU energies (see Figure 4) achieved with the driving systems;

(3) Dynamic Smith model soil parameters: $Q_{p,s}$ = $Q_{p,b}$ = 2.54 mm, J_s = 0.2 s/m and J_b = 0.5 s/m.

Bearing graph relating SRD to blow counts were developed for each given penetration and the identified the SRDs that matched the recorded blow counts obtained by interpolation. The limited frequency of the ENTHRU energy recordings led to the discontinuous profiles shown in Figure 8 that show broadly similar trends to the Alm and Hamre (2001) predictions, although indicating lower 'Global Match' SRDs at most depths below 27 mbgl.

The SRD values back-calculated from signal matching using the alternative two soil models at three penetration depths are also plotted, showing good agreement with the Alm and Hamre (2001) predictions and 'measured' global matches. Table 5 summarises the deduced overall EoD shaft and base components. While the shaft capacities inferred from all three means are compatible, the Continuum model base resistances are higher (≈ $0.6q_c$) than the 0.2 - $0.3q_c$ outcomes from the 'Global Match' and CAPWAP analyses. The uncertainty regarding the base capacity is discussed further in the Appendix.

Figure 9 shows the profiles with depth of the total limiting shaft resistances, τ_s (external plus internal) back-calculated from two signal matching models in comparison with the static (medium-age) profiles predicted by the ICP-05 (sand) combined with the UWA-13 (clay) procedures. Results from the Continuum model show broadly consistent trends for blows Loc1_BN3005 and Loc2_BN3115 over most of the profile, as might be expected due to the similar pile penetrations, CPT resistances and dynamic signals (see Figures 4 and 5). For all three blows, the shaft resistances interpreted from signal matching fall well below the static prediction method profiles which incorporate the 'set-up' developed 14 to 25 days after driving. The Continuum model also yields EoD shaft resistances comparable to the static prediction methods for blows Loc1_BN3005 and Loc2_BN3115, while a more pronounced difference was observed for blow Loc1_BN10.

IMPACT and CAPWAP analyses produce similar shaft resistances for blows Loc1_BN3001 and Loc2_BN3115, with absolute differences limited to around 7 kPa on average over the upper 30 m. For all three blows, a considerable discrepancy is observed between the CAPWAP and IMPACT predictions near the pile tip. Significantly different shaft resistance profiles were also observed within the mixed alternating layer (15-20 mbgl), where the apparent drop in the IMPACT results is consistent with the trend of the CPT measurements.

Marked effects of relative pile tip depth h/R^* are apparent in Figure 9, where h is the distance above the pile tip, R^* is the equivalent radius (=$\left(r_o^2 - r_i^2\right)^{0.5}$). For example, over the depth range of 27-30 m, the mean τ_s from the Continuum model is approximately 150 kPa for Loc1_BN10 when the pile tip was at 30.6 mbgl. After a further 16.5 m of penetration for blow Loc1_BN3001, the τ_s value applying over this depth range reduced to 60 kPa, less than half the earlier value.

Figure 10 plots the distributions of static shaft resistances (internal + external) measured from strain gauges in four compression tests, corresponding to a pile head displacement of *D*/10 (Kolk et al., 2005). Comparison with the τ_s values inferred from signal matching (EoD) indicates that pronounced increases in local resistance occurred over the first two weeks after pile installation, particularly over the lower pile section. For instance, the static test Loc1_CP2 (12-day age) produced a local τ_s of about 1700 kPa near the pile tip, whereas blow Loc1_BN3115, recorded at the same penetrations led to a far lower EoD τ_s of around 550 kPa in the IMPACT analyses. Figure 10 also shows the shaft resistance profiles deduced from the strain gauge measurements made during the long-term static tests Loc2_CP2 (533 ageing days) along with those from the earlier (6-day age) Loc2_CP1. Comparison of τ_s measurements indicate apparent capacity gains over most of the depth ranges, confirming strongly positive shaft resistance ageing effects, except over the 41-43 mblg depth range. This anomaly may be related to the presence of a silty layer at Location 2 (see Figure 2). Further detailed discussion on the static tests is given in the next section.

RELATIONSHIP TO STATIC TESTS

The shaft and base capacities of three 'first-time' constant rate of penetration (CRP, set at 1 mm/min) tests (Loc1_CP1, Loc1_CP2, Loc2_CP1) and one long term re-test (Loc2_CP2) reported by Kolk et al.

(2005) are considered in relation to the dynamic data. No relative movement of the ISC was observed, indicating globally plugging failure modes (Fugro, 1996).

Figure 11 presents pile head force-displacement curves for selected tests. Pile annular base forces were interpreted for Loc1_CP1 and Loc1_CP2 by Kolk et al. (2005) from strain gauges fixed around 0.38 m above pile tip; instruments located closer to the toe did not survive driving. The two tests showed essentially identical annular base capacities (Q_{ba}). However, it should be noted that estimating the annular base resistances of open pipe piles from strain gauges is problematic due to both intense stress concentrations close to the tip and the uncertain contribution of internal shaft friction. Fully independent double-wall measurements are required to independently assess the outer shaft, inner shaft, and annular base resistances of pipe piles during static testing, see for example Han et al. (2020).

Equivalent strain-gauge measurements of pile force distributions with depth were unavailable for Loc2_CP1 and Loc2_CP2 due to gauge damage during re-driving. Following Rimoy et al. (2015), it is assumed that similar base capacities applied to the Loc2_CP1 and Loc2_CP2 tests despite their different ages. Any unaccounted for growth in annular base resistance would to lead overestimation of the shaft capacity set-up factors discussed in the next section.

Loc2_CP2 developed a pile head load of around 26 MN, far greater that in the earlier age tests, and had to be terminated after reaching a displacement of 0.055 m when the load reached the system's safe structural capacity. The load-displacement data were extrapolated using the alternative routines suggested by Hansen (1963), Chin (1970), and Decourt (1999), yielding the pile capacities in the range 32.8-34.2 MN, with an average of 35.3 MN at the 10%*D* pile head displacement, as shown in Figure 11 (b). These extrapolation approaches could be unconservative if any inflection point developed before reaching 10%*D*, as occurred at the early age compression tests. Table 6 summarises the static pile shaft and annular base capacities, Q(ASC), interpreted for selected compression tests, together with the ICP-05 and Unified-20 predictions. As expected from Lehane et al. (2000), the total capacities from those two methods are in good agreement.

ASSESSMENT OF TIME EFFECTS ON PILE CAPACITY

Pile set-up factors from dynamic tests are normally defined as the ratio of the Beginning of Restrike (BoR) soil resistance, as obtained at some age after driving, to the EoD resistances for the same pile and tip depth. Since dynamic restrike tests were not conducted on the EURIPIDES piles, set-up was gauged by comparing dynamic EoD tests and static tests after ageing, assuming initially that axial static compression capacities can be compared directly with BoR resistances.

The first comparison made for the Location 1 pile requires careful consideration, since the EoD blow employed (Loc1_BN10) originates from the 10th dynamic blow applied after the static test Loc1_CP1 had been performed. As discussed earlier, the resistance back-calculated from Loc1_BN10 is the best available proxy for the pile's EoD resistance prior to the ageing and static testing applied at that depth. The other two blows considered (Loc1_BN3001 and Loc2_BN3315) provided unambiguous EoD records for their respective medium-term static compression tests at close depths. The outcome of analysing the latter blow also defined the initial capacity from which set-up was calculated based on the Location 2 long-term retest.

The effects of time on pile shaft capacities in the present study were assessed by computing both the ratio of Q_s(ASC)/ Q_s(EoD) and the ratios of Q_s(ASC) to the capacities predicted by the ICP-05 methods Q_s(ICP), which are expected to predict the medium-term capacities available at around 10 to 30 days after installation. Although an apparent enhancement in pile annular base capacity (Q_{ba}) over time may be inferred from comparing the dynamic analysis results with the static measurements (see Table 5 and 6), it has to be recalled that the displacements developed in dynamic blows fall far below the *D*/10 levels at which static capacity was defined. Considerable uncertainty also exists regarding the determination of Q_{ba} from dynamic analysis, as noted in the related sensitivity analysis. Further investigation to the ageing effects on Q_{ba} is beyond the scope of the present study.

Figure 12 plots the ratios of Q_s(ASC)/ Q_s (EoD) for the pile shaft resistances. Maximum, minimum and average values of three extrapolation method for the 533-day Loc2_CP2 test are also plotted. Assuming no gain in base resistance led to a maximum set up ratio (from the Smith model) of 3.4. The Continuum model and ‘Global Match’ trends generally lie close together, with both falling below that from the Smith model SRDs. In general, all tests manifested a marked shaft capacity growth with time, giving 50% $\pm$ 25% growth per log time cycle in the medium to long term, as noted by Chow et al. (1998), Axelsson (2000), Konig and Grabe (2006) and Rimoy et al (2015). Cathie et al. (2022) present trends established from dynamic testing on far larger diameter offshore piles. They show that similar trends appear to apply to larger diameter (2.5 to 3.5 m diameter) piles at ages up to around 20 days, but they suggest less longer-term set-up growth than has been observed with smaller diameter onshore piles.

Figure 13 shows the shaft capacity ratios of Q_s(t)/ Q_s(ICP) on semi-logarithmic axes. The ratios plotted for a nominally ‘1 day’ age are interpreted from pile dynamic analyses employing the Continuum, Smith and ‘Global Match’ methods, whereas the later age ratios come from the compression tests. Also plotted in Figure 13 are trends previously proposed by Rimoy et al. (2015) and Yang et al. (2017) from previous tension testing studies on smaller piles. The Q_s(t)/ Q_s(ICP) shaft ratios immediately after driving are in the range of 0.5-0.7, (on average 0.65) increasing gradually to around 1.0 after around 10 days, matching the nominal ICP-05 target age after driving. It is of great interest that the capacity in long term (533 ageing day) tests is nearly double the ICP-05 prediction, indicating a strong ageing effect on pile capacity for the 763 mm diameter steel pile. As noted above, larger offshore piles appear to show lower long term set-up ratios (Cathie et al. 2022).

While no side-by-side static and dynamic tests were performed at exactly the same ages, the static and dynamic shaft capacity follow compatible trends. Extrapolation of the Figure 12 and Figure 13 trends back to 1-day ages indicates that dynamic EoD capacity is broadly equivalent to the static resistance available within the first day of driving. The dynamic EoD base capacities are on average equivalent to 57% of the ICP-05 sand predictions. If normalised by Unified-20 calculations, the EoD shaft and base capacities amount to 70% and 47% of the respective predictions.

SUMMARY & CONCLUSIONS

This paper presents a new interpretation of previously unpublished instrumented driving data from the EURIPIDES project, relating these to companion static compression tests on strain-gauged piles and so inferring relationships between dynamic and static resistances. Signal matching analyses employed to back-analyse the dynamic signal records considered two distinct pile-soil interaction models to simulate the dynamic soil resistance response. 'Global Match' analyses were also carried out in the present study to estimate pile capacities. The main findings are summarised as follows:

- The Continuum model analyses produce, on average, 20% higher pile shaft capacities than Smith modelling with equivalent input parameters, demonstrating broad compatibility between the two approaches.
- The soil columns inside open-ended piles have a pronounced effect on signal matching performed with the Continuum model and could result in differences in the predicted soil resistance to driving. Best quality signal matches were obtained when the interior local shaft resistance was set equal to 10-20% of the external shaft resistance. Further theoretical and experimental research is required to investigate this shaft resistance split.
- Analyses of four static compression tests in relation to End of Driving resistances confirm strong and positive effects of ageing time on shaft capacity.
- Shaft capacity set up factors of 1.4 to 1.7 on average were interpreted after 6 to 12 days and a ratio of 3 extrapolated from a 533-day age test falls within the 50% (±25%) per log cycle medium-to-long term trends reported by others and match those established previously in independent tension testing studies. However, it is recognised that larges piles may show less marked long-term set-up.
- While side-by-side static and dynamic tests were not performed at exactly comparable ages, the post-driving static measurements indicate that dynamic EoD capacities are broadly equivalent to the static capacities expected within the first day of driving and amount to, on average, 65% and 57% of the medium-age shaft and base resistances respectively, as predicted by the ICP-05 sand method.

ACKNOWLEDGEMENTS

This study formed part of the PAGE (Pile ageing in sands) JIP which was executed by a consortium led by Cathie with partners GCG and Prof. Richard Jardine. The JIP was sponsored by BP, DEME Offshore, EnBW, Equinor, Jan de Nul, Scottish Power Renewables, Van Oord and Ørsted, and supported by a technical review panel consisting of Jens Bergan-Haavik (DNV GL), Dr Oswald Klingmuller (GSP), Dr Neil Morgan (Lloyds Register), Dr Frank Rausche (Pile Dynamics Inc) and Prof. David White (University of Southampton). Their support is gratefully acknowledged. The authors wish to express their gratitude to Professor M. F. Randolph and Peter Middendorp for granting access to IMPACT and Allwave-PDP software respectively. The first author is funded by a Skempton scholarship of the Department of Civil & Environmental Engineering at Imperial College and the China Scholarship Council (CSC).

APPENDIX Sensitivity of signal matching to input parameters using the Continuum model

Influence of stiffness profile

As previously discussed, the Continuum model requires a stiffness profile as an input. To account for soil nonlinearity and the associated stiffness degradation, values of operational shear modulus are commonly adopted as a proportion of G_{max}. A single operational shear modulus is difficult to assign, as shear strain levels vary steeply with radial distance from the pile (Loukidis et al., 2008). Figure A-1 shows the effects on the external shaft resistance $\tau_{s,out}$ characteristics of a single soil-pile element from 10 m depth of varying $G_{o,out}$ from $0.1G_{max}$ to $0.5G_{max}$ while keeping other parameters (α = 0.3, β = 0.2) constant. The resistances from different soil model components were calculated as summarised in Table 3. As shown in Figure A-1 (a), reducing $G_{o,out}$ leads to considerable change in the computed soil displacement $w_{s,s}$ which in turn affects the curves of inertial and viscous resistances in Figure A-1 (b)-(c). Inertial dashpot response is observed to dominate the initial response of pile-soil interaction in the Continuum model; once the maximum inertial resistance is reached, the higher the $G_{o,out}$, the more pronounced is the decay in inertial resistances, indicating its less contribution to total resistance during unloading phase. Given that $G_{o,out}$ theoretically has no impact on the definition of viscous dashpot, the difference observed for curves in Figure A-1 (c) is mainly due to the $w_{s,s}$ variations caused by different $G_{o,out}$, as noted earlier. Although different components (spring and dashpots) in Continuum model are only activated at specific time intervals according to their definition, Figure A-1 depicts the evolution of spring and dashpot resistance for the complete duration of a hammer impulse.

Figure A-2 shows the influence of the base operational shear modulus $G_{o,b}$ on the dynamic response of the pile tip. All other parameters are held fixed while $G_{o,b}$ is varied from $0.2G_{max}$ to $0.6G_{max}$. The base response is considered by a spring and inertial dashpot as listed in Table 3. Unlike the shaft Continuum model, no viscous dashpot is incorporated in the base model. Increasing $G_{o,b}$ leads to a higher mobilised total resistance. For $G_{o,b} = 0.6G_{max}$, the total resistance exceeds the assumed q_b before the plastic slider is engaged after a base displacement of 1.4 mm. However, when $G_{o,b} = 0.2G_{max}$, the total resistance fails to meet the assumed q_b at any time, implying the plastic slider component is not engaged and therefore has no effect on the $F_{u,c}$. In this case, adopting a higher q_b has no impact on $F_{u,c}$ but could still be reported as a higher 'dynamically matched' pile base capacity. Care is needed to ensure that the values of $G_{o,b}$ employed lead to meaningful pile base capacities.

Influence of the internal Soil Column

Considering next the influence of the ISC during driving, Figure A-3 shows an example of matching the F_u using three approaches for addressing the 30 m long ISC recorded during blow Loc1_BN10: a) Smith lumping of the internal and external resistance together; b) Continuum modelling the ISC; c) Continuum lumped modelling of the internal and external resistances together. It should be noted that all the sensitivity analyses for the ISC are conducted with IMPACT (i.e. both the Continuum and the Smith model analyses). Their corresponding matching quality index M_q are also given. Note that an identical distribution of total shaft resistances (external + internal) and base resistance are assumed in those three approaches. It is evident that lumping the external with internal response has a significant effect on the computed $F_{u,c}$, particularly on the peak values of $F_{u,c}$, even when using an identical Continuum model.

Recognising that ISC resistance has an important effect on signal matching, it is necessary to quantify the internal resistance. Although the ratio of internal to external shaft friction ($\tau_{s,in}/\tau_{s,out}$) may vary along the pile length, constant ratios were adopted for the analysis of the same blow as suggested by Doherty et al., (2020). Values of $\tau_{s,in}/\tau_{s,out}$ from zero to 0.5 were assumed while maintaining the total resistances ($\tau_{s,in} + \tau_{s,out}$) identical. The operation shear moduli for external soil ($G_{o,out}$) is a constant of $0.5G_{\max}$ to account for soil non-linearity and the associated stiffness degradation, while the moduli for ISC $G_{o,in}$ is certain a proportion of $G_{o,out}$ ($G_{o,in}$ = $0.3G_{o,out}$). Figure A-4 shows how changes in $\tau_{s,in}$ affect the computed $F_{u,c}$ and w_p traces. The peak $F_{u,c}$ values and final pile sets increase with $\tau_{s,in}/\tau_{s,out}$ and taking $\tau_{s,i}/\tau_{s,e} = 0.1$ and 0.2 provides the best M_q matches. Related studies shows that ISC shear modulus has a far less significant effect on the signal matching quality and outcomes.

While the sensitivity study identified how the main input variables affect outcomes, the conclusions are likely to be case-specific and may require re-evaluation for other piles, sites or even blows.

REFERENCES

Allnamics (2015). AllWavePDP User's reference manual, Allnamics BV. (Draft for review and comment.)

Alm, T., and Hamre, L. (2001). Soil model for pile driveability predictions based on CPT interpretations. In: proceeding of the 15th International Conference on Soil Mechanics and Foundation Engineering. Istanbul, Turkey, pp. 1297-1302.

Axelsson, G. (2000). Long term set-up of driven piles in sand. PhD thesis, Royal Institute of Technology, Stockholm, Sweden.

Hansen, J. B. (1963). Discussion of Hyperbolic Stress-Strain Response: Cohesive Soil. By Robert L. Kondner. J. Soil Mech., Found. Div., ASCE, 89(4), 241-242.

Brucy, F., Meunier, J. and Nauroy, J. F. (1991). Behaviour of pile plug in sandy soils during and after driving. Proc. 23rd Offshore Technology Conf., Houston, 145–154.

Buckley, R. M. (2018). The axial behaviour of displacement piles in chalk. PhD Thesis, Imperial College London, London, UK.

CAPWAP Manual (2006). Pile Dynamics, Inc., Cleveland Ohio, USA.

Cathie, D., Jardine, R. J, Silvano, R., Kontoe, S. and Schroeder. F (2022). Pile setup in sand – the "PAGE" joint industry project. Keynote paper. Proc. 11th International Conference on Stress Wave Theory and Design and Testing Methods for Deep Foundations. Rotterdam. September 2022. In Press.

Chin F. K. (1970). Estimation of the ultimate load of piles not carried to failure. Proc. 2nd Southeast Asian Conf. on Soil Eng., Singapore: 81-92

Cho, C. W., Lee, M. W., and Randolph, M. F. (2000). "Set-up considerations in wave equation analysis of pile driving." Proc., Sixth Int. Conf. on the Application of Stress Wave Theory to Piles, 41–46.

Chow, F. C., Jardine, R. J., Brucy, F., and Nauroy, J. F. (1998). Effects of time on capacity of pipe piles in dense marine sand. Journal of Geotechnical and Geoenvironmental Engineering, 124(3), 254-264.

Coyle, H. M., and Gibson, G. C. (1970). Empirical damping constants for sands and clays. Journal of the Soil Mechanics and Foundations Division, 96(3), 949-965.

Decourt, L. (1999). Behavior of foundations under working load conditions. 11th Pan-American Conference on Soil Mechanics and Geotechnical Engineering, Foz do Iguaçu, 4, 453-488.

Deeks, A. J., and Randolph, M. F. (1995). A simple model for inelastic footing response to transient loading. International journal for numerical and analytical methods in geomechanics, 19(5), 307-329.

Doherty, J.P., and Randolph, M.F. and Schneider, J.A. (2020). Analyzing the driving performance of pile foundations using data driven models. In 4th International Symposium on Frontiers in Offshore Geotechnics, 664-673.

Fellenius, B. H. (1988). Variation of CAPWAP results as a function of the operator. In Proc. Of the 3rd Int. Conf. on the Application of Stress Wave Theory to Piles, Ottawa, Canada, 814-825.

Fugro (1996). EURIPIDES database report, Vols 1–5. Leidschendam, The Netherlands: Fugro BV.

Galvis-Castro, A. C., Tovar-Valencia, R. D., Salgado, R., and Prezzi, M. (2019). Effect of loading direction on the shaft resistance of jacked piles in dense sand. Géotechnique, 69(1), 16-28.

Gavin, K. G., Igoe, D. J. P., and Kirwan, L. (2013). The effect of ageing on the axial capacity of piles in sand. Proceedings of the Institution of Civil Engineers-Geotechnical Engineering, 166(2), 122-130.

Han, F., Ganju, E., Prezzi, M., Salgado, R., and Zaheer, M. (2020). Axial resistance of open-ended pipe pile driven in gravelly sand. Géotechnique, 70(2), 138-152.

Jardine, R., Chow, F., Overy, R., and Standing, J. (2005). ICP design methods for driven piles in sands and clays (Vol. 112). London: Thomas Telford.

Kolk, H.J., Baaijens, A.E., and Vergobi, P. (2005). Results of axial load tests on pipe piles in very dense sands: The EURIPIDES JIP. Frontiers in Offshore Geotechnics, Taylor & Francis, London, 661 – 667.

Konig, F., and Grabe, J. (2006). Time dependant increase of the bearing capacity of displacement piles. Piling and Deep Foundations. In Conference Proceedings, DFI EFFC, Amsterdam (pp. 709-717).

Lehane, B. M., Li, Y., and Williams, R. (2013). Shaft capacity of displacement piles in clay using the cone penetration test. Journal of Geotechnical and Geoenvironmental Engineering, 139(2), 253-266.

Lehane, B. M., Schneider, J. A., and Xu, X. (2005). The UWA-05 method for prediction of axial capacity of driven piles in sand. Frontiers in offshore geotechnics: ISFOG, 683-689.

Lehane, B., Liu, Z., Bittar, E., Nadim, F., Lacasse, S., Jardine, R. J., ... and Morgan, N. (2020). A new 'unified' CPT-based axial pile capacity design method for driven piles in sand. In 4th International Symposium on Frontiers in Offshore Geotechnics (pp. 463-477). American Society of Civil Engineers.

Liang, R. Y., and Sheng, Y. (1993). Wave equation parameters from driven-rod test. Journal of geotechnical engineering, 119(6), 1037-1057.

Likins G, DiMaggio J, Rausche F and Teferra W (1992) A solution for high damping constants in sands. In Application of Stress-Wave Theory to Piles (Barends FBJ (ed.)). Balkema, Rotterdam, the Netherlands, pp. 117–120.

Litkouthi, S., and Poskitt, T. J. (1980). Damping constants for pile driveability calculations. Geotechnique, 30(1), 77-86.

Lunne, T., and Christoffersen, H. P. (1983). Interpretation of conepenetrometer data for offshore sands."InProc., 15th AnnualOffshore Technology Conf., 181–188. Houston: Offshore TechnologyConference.

Matsumoto, T., and Takei, M. (1991). Effects of soil plug on behaviour of driven pipe piles. Soils and Foundations, 31(2), 14-34.

Middendorp P. (2015). RE: Allwave-DLT signal match quality assessment – Personal Communication.

Middendorp, P., and van Weel, P. (1986). Application of characteristic stress wave method in offshore practice. In Proceedings of the 3rd International Conference on Numerical Methods in Offshore Piling, Nantes, 6-18.

Ng, K. W., and Sritharan, S. (2013). Improving dynamic soil parameters and advancing the pile signal matching technique. Computers and Geotechnics, 54, 166-174.

Novak, M., Aboul-Ella, F., and Nogami, T. (1978). Dynamic soil reactions for plane strain case. Journal of the Engineering Mechanics Division, 104(4), 953-959.

Randolph M. F. (2008). IMPACT – Dynamic analysis of pile driving, Manual

Randolph, M. F. (1987). Modelling of the soil plug response during pile driving. Proc. 9th SE Asian Geotech. Conf., Bangkok, vol 2, pp. 6.1–6.14.

Randolph, M. F. (2003). Science and empiricism in pile foundation design. Géotechnique, 53(10), 847-875.

Rausche, F., Likins, G. and Liang, L. (2010). Static and dynamic models for CAPWAP signal matching. In Art of foundation engineering practice, pp. 534–553. West Palm Beach, FL, USA: American Society of Civil Engineers.

Rausche, F., Moses, F., and Goble, G. G. (1972). Soil resistance predictions from pile dynamics. Journal of the soil mechanics and foundations division, 98(9), 917-937.

Rimoy, S., Silva, M., Jardine, R., Yang, Z. X., Zhu, B. T., and Tsuha, C. D. H. (2015). Field and model investigations into the influence of age on axial capacity of displacement piles in silica sands. Géotechnique, 65(7), 576-589.

Robertson, P. K., and Wride, C. E. (1998). Evaluating cyclic liquefaction potential using the cone penetration test. Canadian geotechnical journal, 35(3), 442-459.

Salgado, R., Loukidis, D., Abou-Jaoude, G., and Zhang, Y. (2015). The role of soil stiffness non-linearity in 1D pile driving simulations. Géotechnique, 65(3), 169-187.

Schneider, J. A., and Harmon, I. A. (2010). Analyzing drivability of open-ended piles in very dense sands. DFI Journal-The Journal of the Deep Foundations Institute, 4(1), 32-44.

Simons, H. A. and Randolph, M. F. (1985). A new approach to one dimensional pile driving analysis. Proceedings of the 5th international conference on numerical methods in geomechanics (eds T. Kawamoto and Y. Ichikawa), pp. 1457–1464. Nagoya, Japan: Balkema.

Smith, E. A. L. (1960). Pile-driving analysis by the wave equation. Journal of the soil mechanics and foundations division, 86(4), 35-61.

Xu, X., Schneider, J. A., and Lehane, B. M. (2008). Cone penetration test (CPT) methods for end-bearing assessment of open-and closed-ended driven piles in siliceous sand. Canadian geotechnical journal, 45(8), 1130-1141.

Yang, Z. X., Guo, W. B., Jardine, R. J., and Chow, F. (2017). Design method reliability assessment from an extended database of axial load tests on piles driven in sand. Canadian Geotechnical Journal, 54(1), 59-74.

Zuidberg H.M., and Vergobbi P. (1996). EURIPIDES, load tests on large driven piles in dense silica sands. Proc. 28th Offshore Technology Conference, Houston, Texas, Vol. 1, 193 – 206.

TABLES

Table 1 Main characteristics of the two testing piles

	Test piles	
	Instrumented section	Add-on section
Initial length at Location 1 / *L* (m)	27	22
Initial length at Location 2 / *L* (m)	26.9	21.6
Outer diameter / *D* (mm)	763.1	763.6
Wall thickness / w_t (mm)	35.55	41.8
Steel cross section / *A* (m^2)	0.0812	0.0948
Young's modulus/ *E* (Mpa)	214569	214569
Dry weight per unit length / W (kN/ml)	6.39	7.60
Equivalent mass density / ρ (Mg/m^3)	7.86	8.02
Impedance / *Z* (kNs/m)	3929	3895
Steel grade	EN460	EN460

Table 2 The selected dynamic blows and static tests

Location	Blow No.	Dynamic blow depth (m)	Static loading sequences	Depth for near static tests (m)	Static tests No.	Pile ageing days
1	Loc1_BN10	30.6	C-T	30.5	Loc1_CP1	7
	Loc1_BN3001	45.9	C-T-R-C-T	47	Loc1_CP2	12
2	Loc2_BN3315	46.23	C-T-R-C	46.7	Loc2_CP1	6
	Loc2_BN3315	46.23	C-T	46.9	Loc2_CP2	533

Notes: C = Compression tests; T = Tension tests.

R = Reloading intended to bring piles into virgin position

Table 3 Soil resistance models employed in this study

<table>
<tr><th colspan="3">Models and their Components</th><th>Mathematical expression</th><th>Variable</th><th>Curve shape</th><th>Schematical model</th></tr>
<tr><td rowspan="6">Continuum model

(Simons and Randolph, 1985; Deeks and Randolph, 1995)</td><td rowspan="4">Shaft</td><td>Spring</td><td>$\frac{G}{D}w_{s,s}$</td><td>D, G</td><td>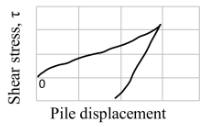</td><td rowspan="4">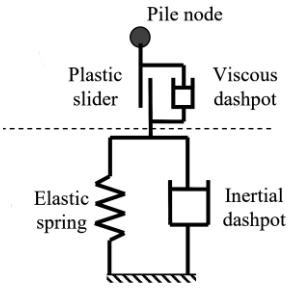</td></tr>
<tr><td>Radiation dashpot</td><td>$\sqrt{G\rho_s}v_{s,s}$</td><td>G, ρ_s</td><td>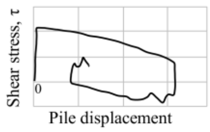</td></tr>
<tr><td>Viscous dashpot</td><td>$\tau_s\alpha\left(\frac{\Delta v}{v_{ref}}\right)^{\beta}$</td><td>$\alpha, \beta$</td><td>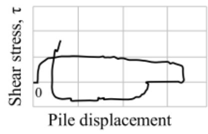</td></tr>
<tr><td>Plastic slider</td><td>τ_s</td><td>-</td><td>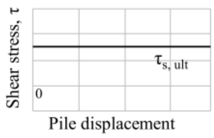</td></tr>
<tr><td rowspan="2">Base</td><td>Spring</td><td>$\frac{2GD}{1-v}w_{s,b}$</td><td>G, v, r_0</td><td>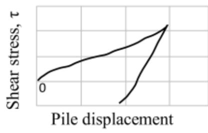</td><td rowspan="2">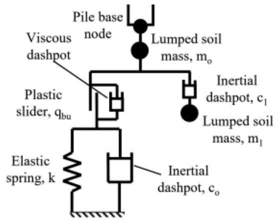</td></tr>
<tr><td>Radiation dashpot</td><td>$\frac{0.8D^2}{1-v}\sqrt{G\rho_s}v_{s,b}$</td><td>$G, \rho_s, r_0$</td><td>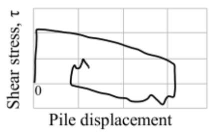</td></tr>
<tr><td rowspan="4">Smith model

(Smith, 1960)</td><td rowspan="2">Shaft</td><td>Spring</td><td>$\tau_s Min\left(1,\frac{w_{p,s}}{Q_{p,s}}\right)$</td><td>$Q_{p,s}$</td><td>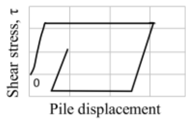</td><td rowspan="2">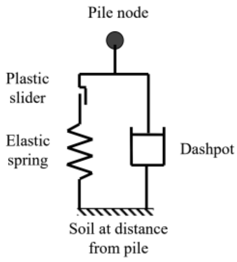</td></tr>
<tr><td>Dashpot</td><td>$\tau_s Min\left(1,\frac{w_{p,s}}{Q_{p,s}}\right)J_s v_{p,s}$</td><td>$J_s, Q_{p,s}$</td><td>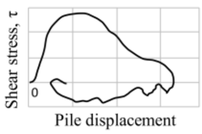</td></tr>
<tr><td rowspan="2">Base</td><td>Spring</td><td>$q_b Min\left(1,\frac{w_{p,b}}{Q_{b,quake}}\right)$</td><td>$Q_{p,b}$</td><td>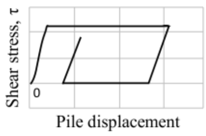</td><td rowspan="2">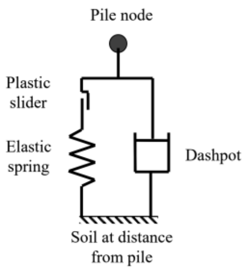</td></tr>
<tr><td>Dashpot</td><td>$q_b Min\left(1,\frac{w_{p,b}}{Q_{p,b}}\right)J_b v_{p,b}$</td><td>$J_b$, $Q_{p,b}$</td><td>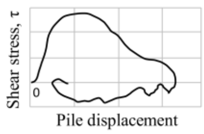</td></tr>
</table>

Table 4 Main input parameters in signal matching

Continuum model	Soil outside pile wall	$G_{o,out}$ (kPa)	0.3 – 0.5 G_{max}
		α	0.25 – 0.45
		β	0.2
	Soil inside pile wall	$G_{o,in}$ (kPa)	0.3 $G_{o,out}$
		$\tau_{s,in}$ (kPa)	0.1 $\tau_{s,out}$
		α	0.25 – 0.45
		β	0.2
	Soil beneath pile base	q_b (kPa)	0.51-0.59q_c
		$G_{o,b}$ (kPa)	0.3 – 0.5 G_{max}
		ρ (Mg/m^3)	2.12
		v	0.5
Smith model	Soil outside pile wall	$Q_{p,s}$ (mm)	1-1.3
		J_s (s/m)	0.1 – 0.7
	Soil beneath pile base	q_b (kPa)	0.3 × q_c
		$Q_{p,b}$ (mm)	1.5-4
		J_b (s/m)	0.3 – 1.3

Table 5 Summary of static pile capacity after end of driving, Q (EoD)

Dynamic blows	Loc1_BN10			Loc1_BN3001			Loc2_BN3315		
	A	B	C	A	B	C	A	B	C
Q_s (MN)	2.2	2.4	2.6	10.1	7.2	9.2	10.9	8.5	11
Q_{ba} (MN)	2.5	0.6	1.2	3.0	1.8	1.3	3.0	1.7	1.2
Q_t (MN)	4.7	3.0	3.8	13.1	9.0	10.5	13.9	10.2	12.2
M_q	2.6%	4.7	-	1.5%	2.8	-	1.1%	2.1	-

Note: A: IMPACT (Continuum model); B: CAPWAP (Smith model);

C: Allwave-PDP (Global Match method)

Table 6 Summary of static pile capacity, Q (ASC)

Static compression tests	Loc1_CP1			Loc1_CP2			Loc2_CP1			Loc2_CP2		
	1	2	3	1	2	3	1	2	3	1	2	3
Q_s (MN)	4.0	4.8	4.4	14.3	14.6	12.8	14.0*	14.9	13.7	29.6*	14.9	13.7
Q_{ba} (MN)	3.9	4.7	5.6	3.9	5.1	6.7	3.9*	5.7	7.2	3.9*	5.7	7.2
Q_t (MN)	7.9	9.5	10.0	18.2	19.7	19.5	17.9	20.6	20.9	33.5	20.6	20.9

Note: 1: Measured; 2: Predicted by ICP-05 (sand) + UWA-13 (clay) method;

3: Predicted by Unified-20 method

* Average extrapolated values for Loc2_CP2 test

LIST OF FIGURES

FIGURES

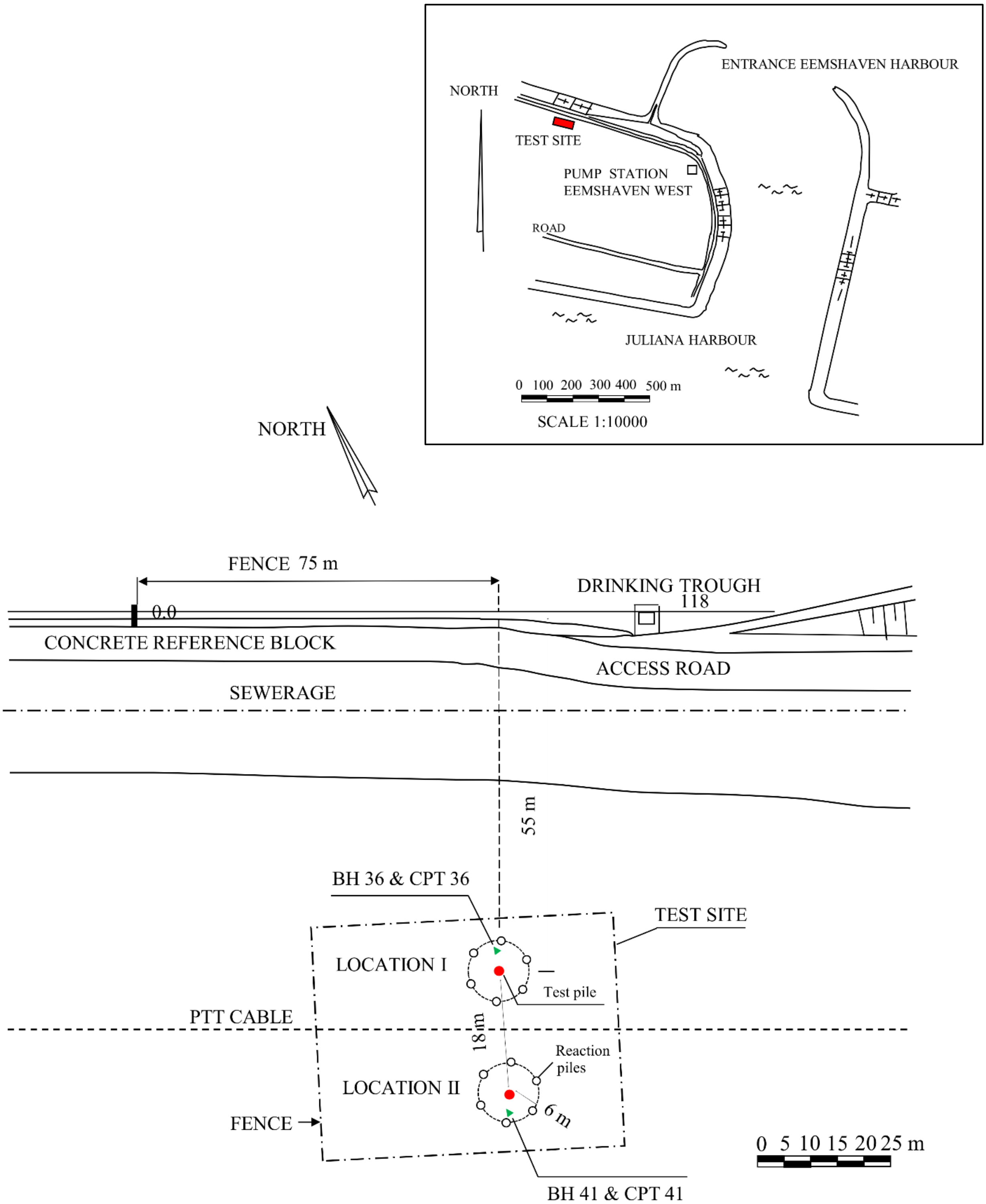

Figure 1 Site plan showing positions of piles and in-situ tests, adapted from Fugro (1996)

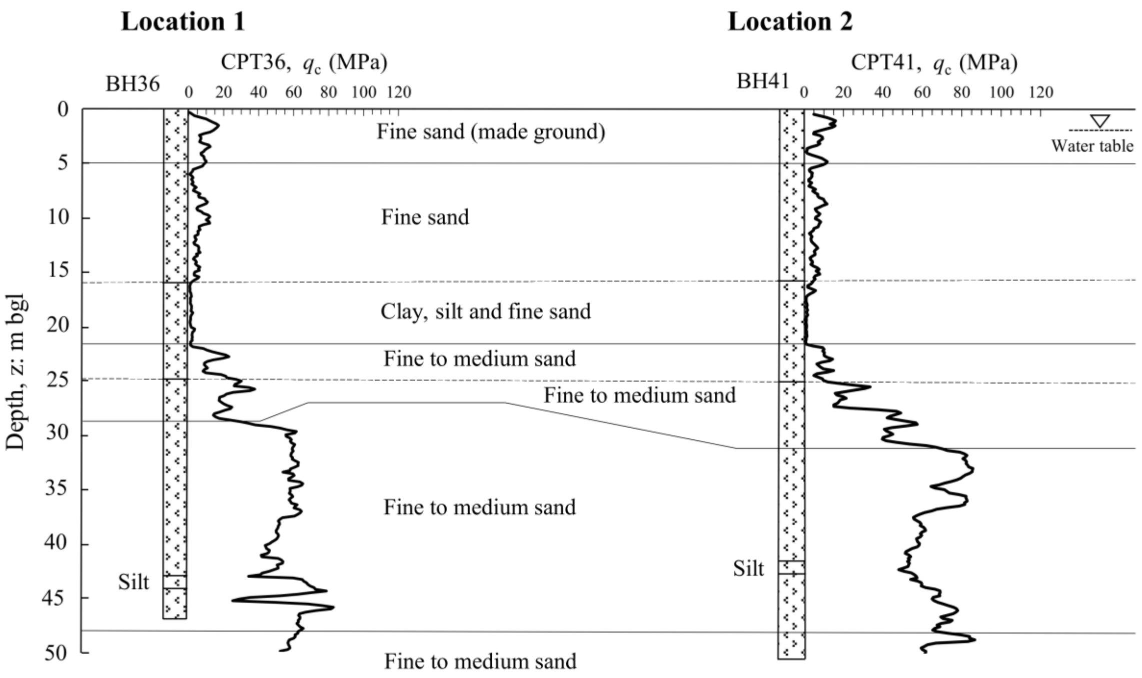

(a)

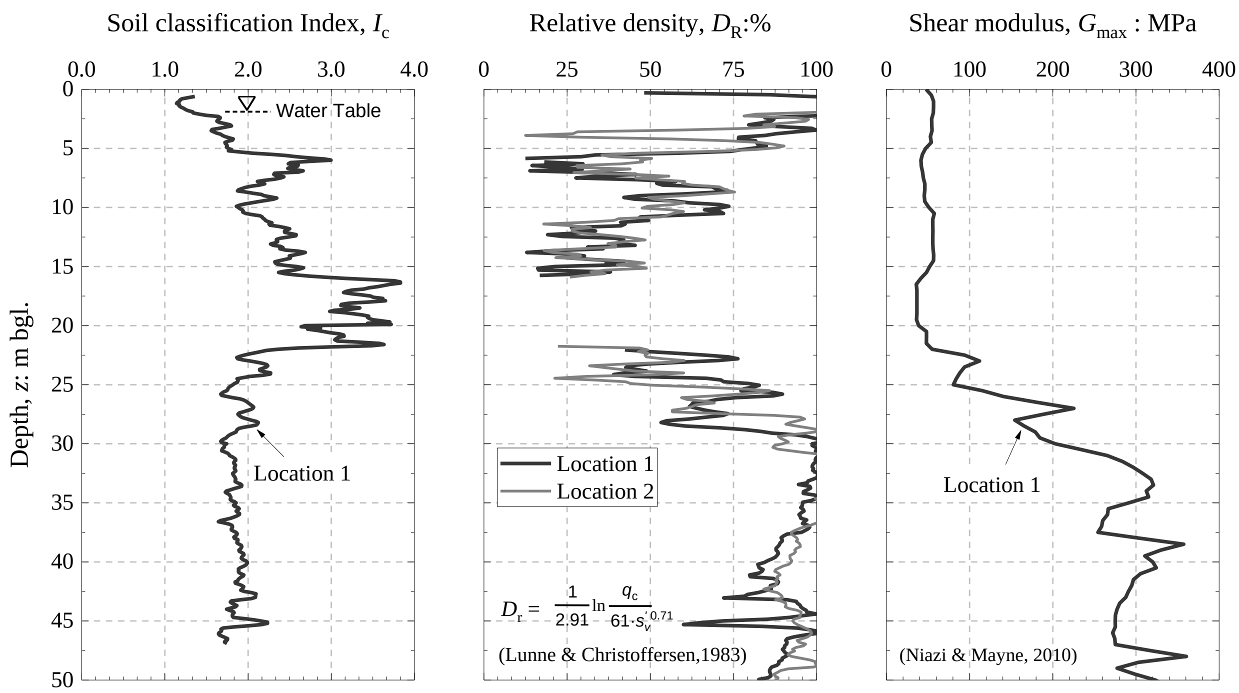

(b)

Figure 2 EURIPIDES site investigation. (a) CPT and soil stratigraphy; (b) profile of Soil classification index, relative density and small-strain shear modulus

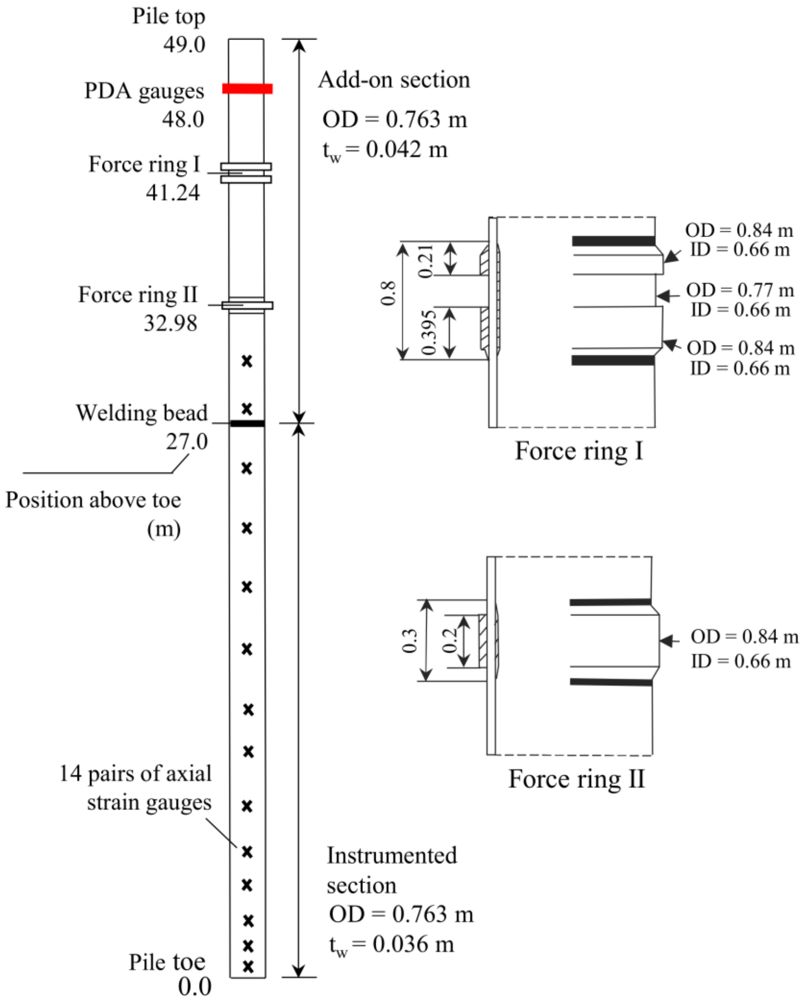

Figure 3 Layout of the test piles and main instruments, adapted from Fugro (1996)

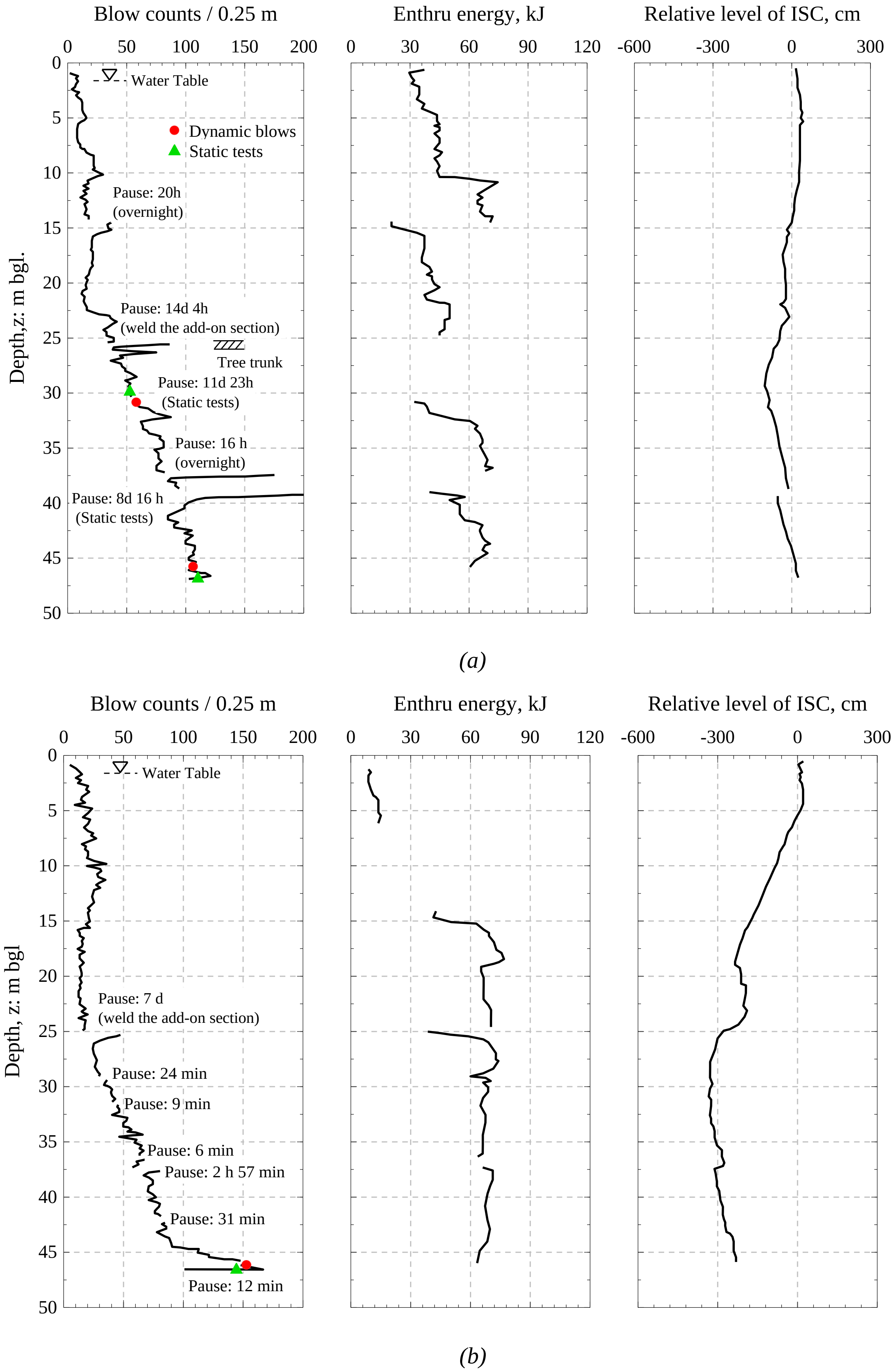

Figure 4 Profiles of blow counts, Enthru energy, plug levels during pile installation; (a) Location 1; (b) Location 2

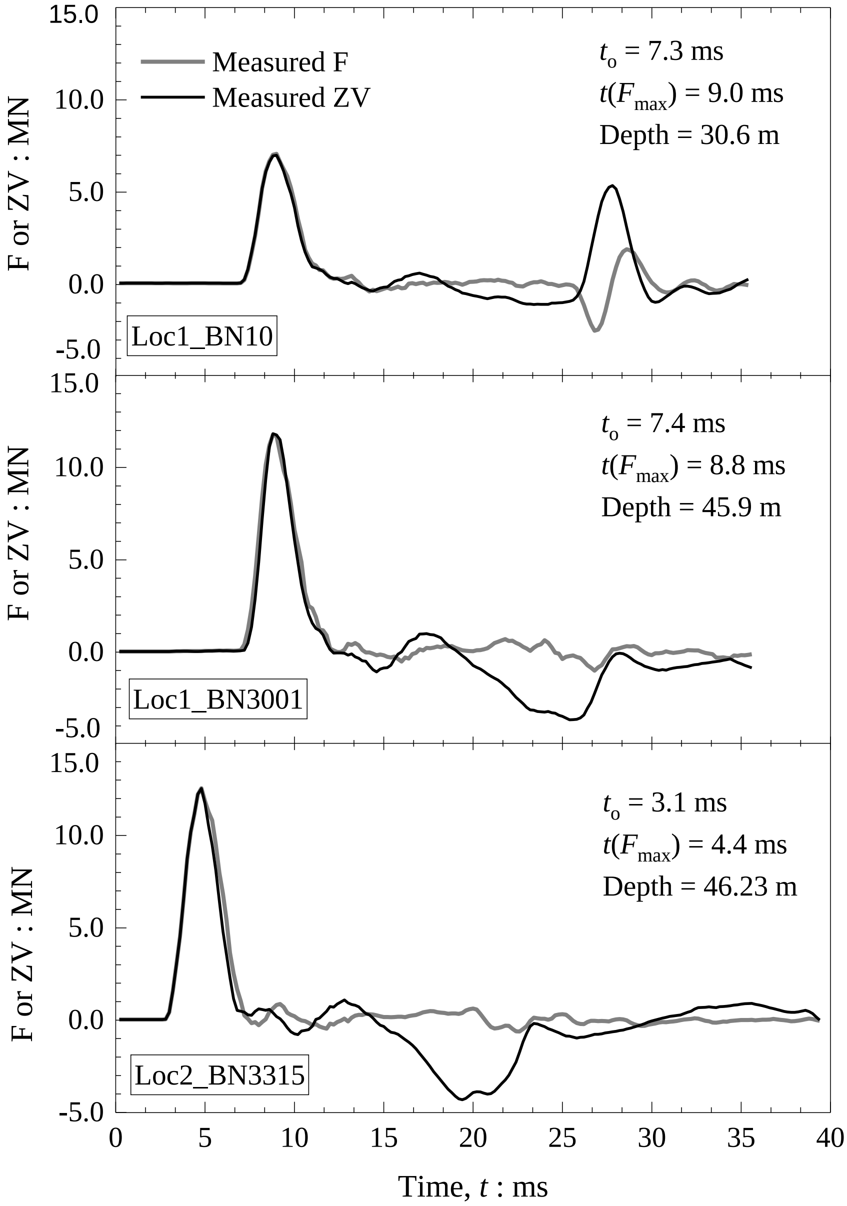

Figure 5 Force and ZV traces of three selected dynamic blows

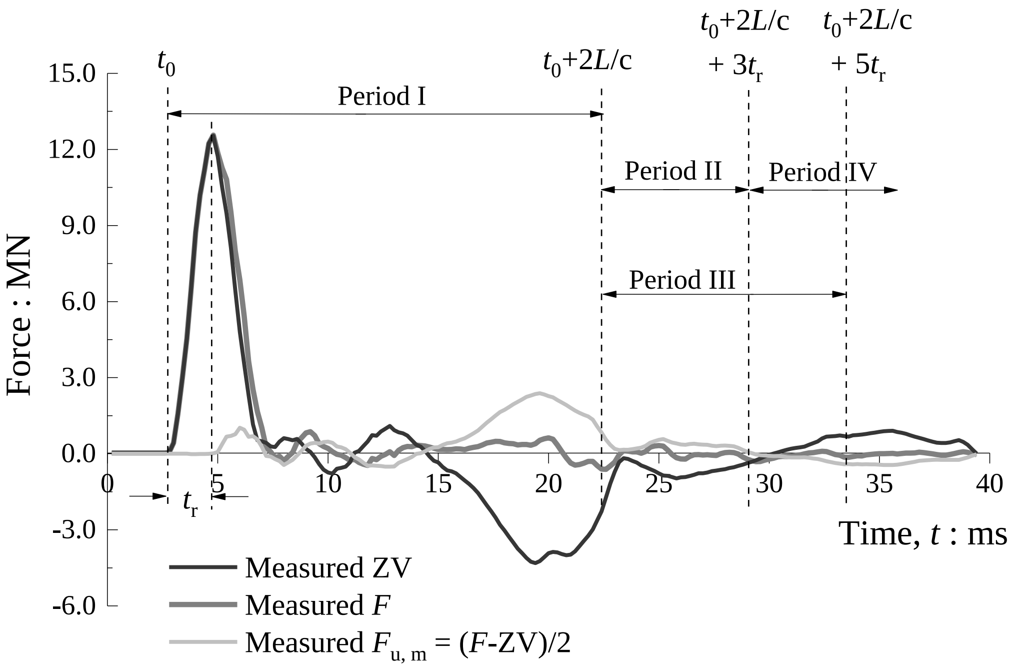

Figure 6 Divisions of periods for match quality assessment

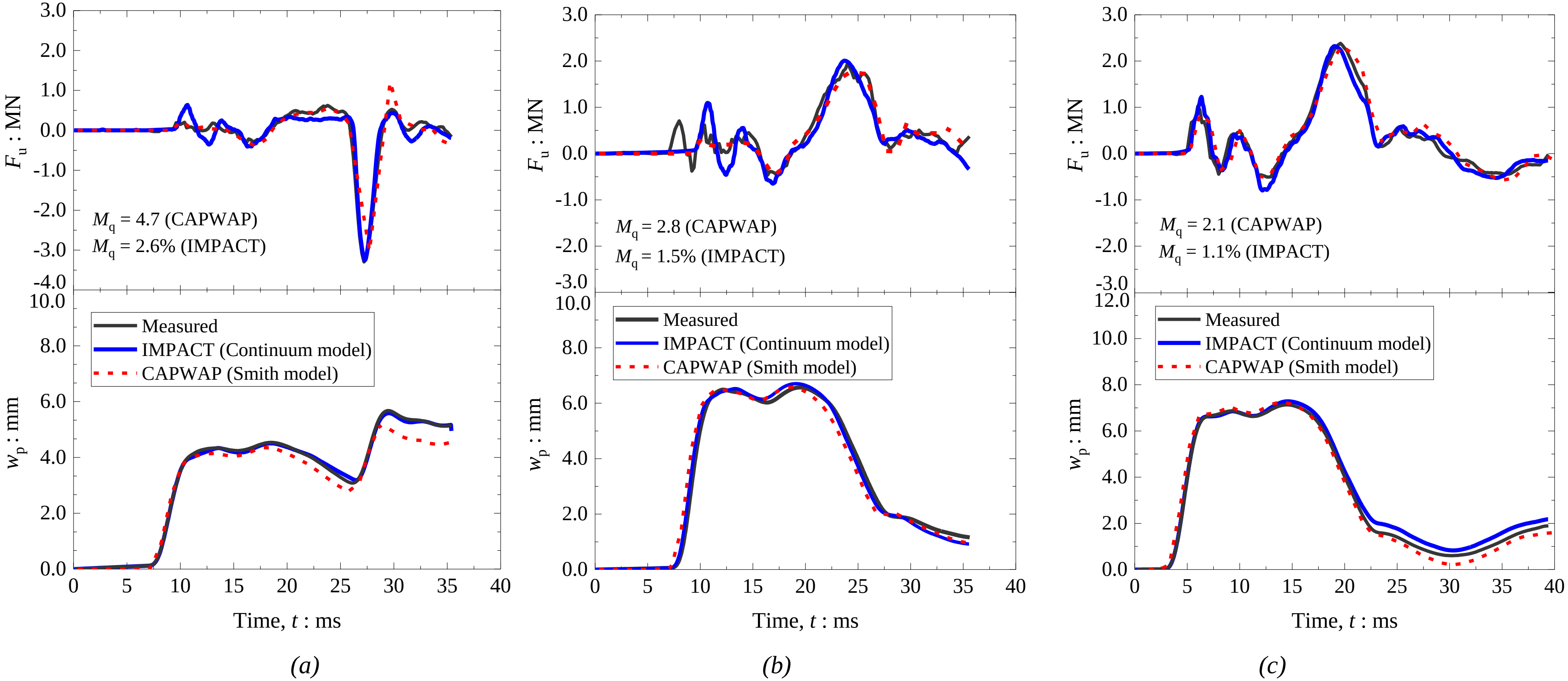

Figure 7 Comparison of measured and computed upward travelling force and pile head displacement for the three blows: (a) Loc1_BN10; (b) Loc1_BN3001; (c) Loc2_BN3115

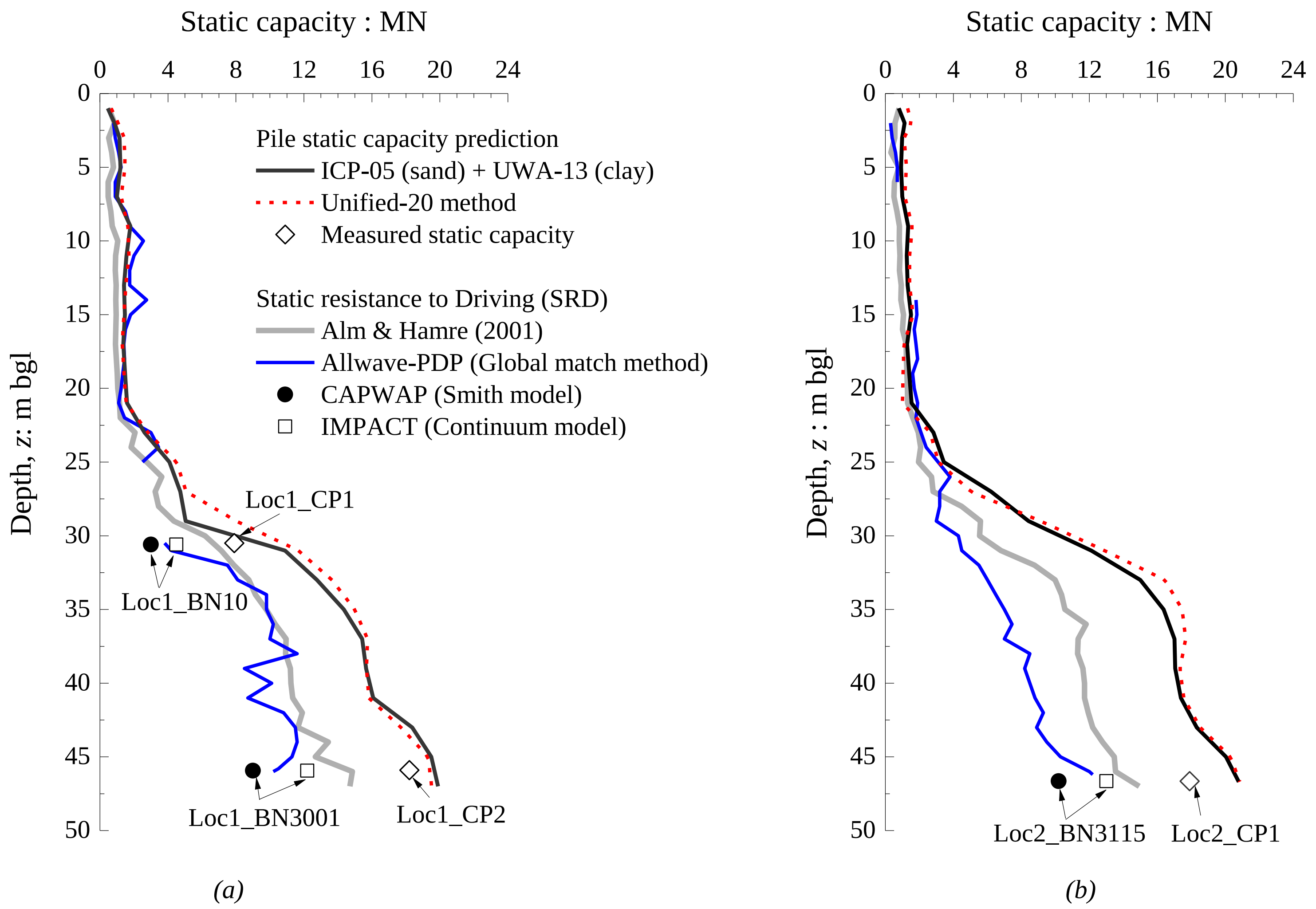

Figure 8 Comparison between predicted and back-calculated static resistance to driving (SRD) and pile static capacity: (a) Location 1; (b) Location 2

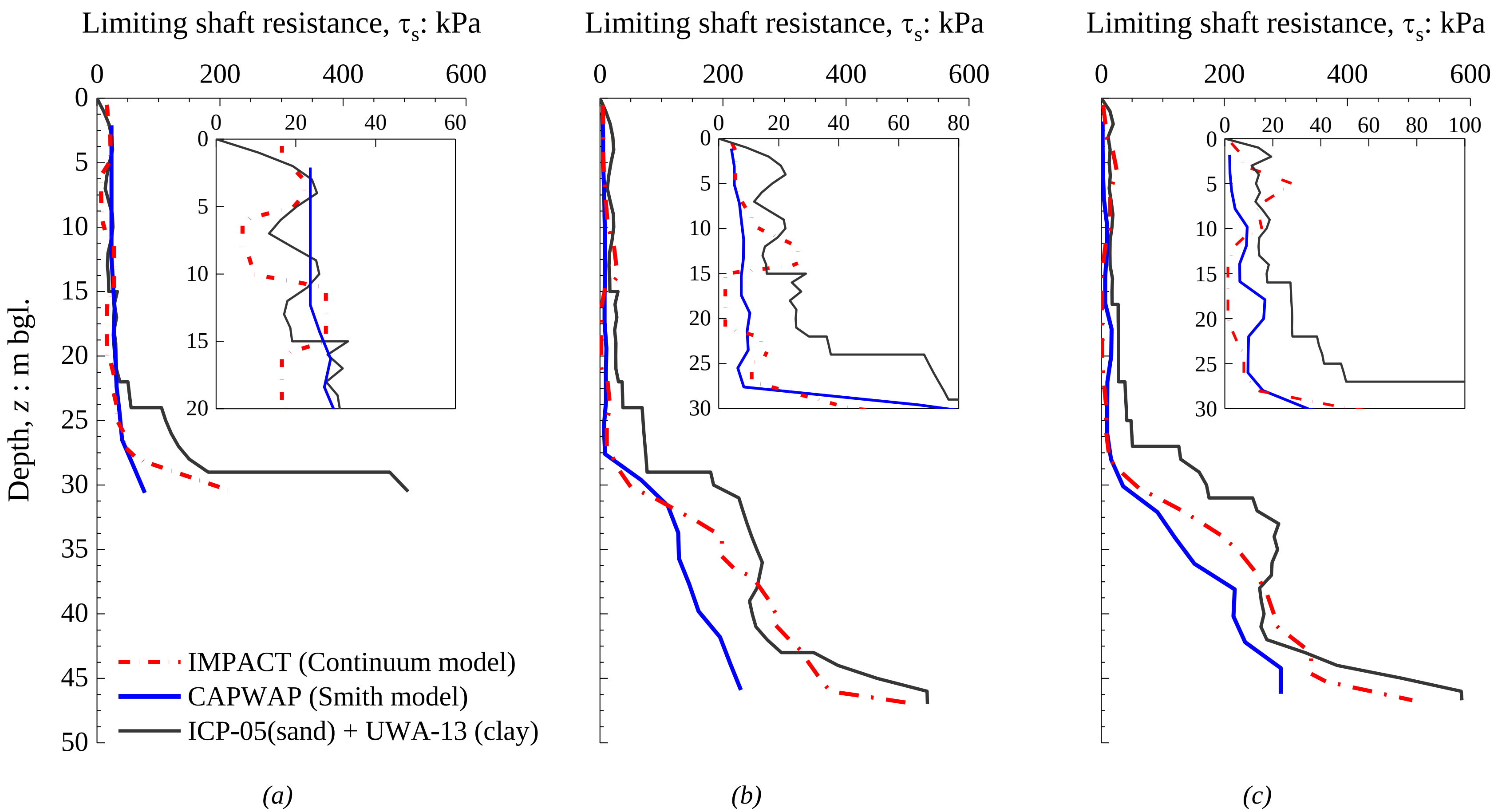

Figure 9 Comparison of shaft resistance distribution at EoD: (a) Loc1_BN10; (b) Loc1_BN3001; (c) Loc2_BN3115

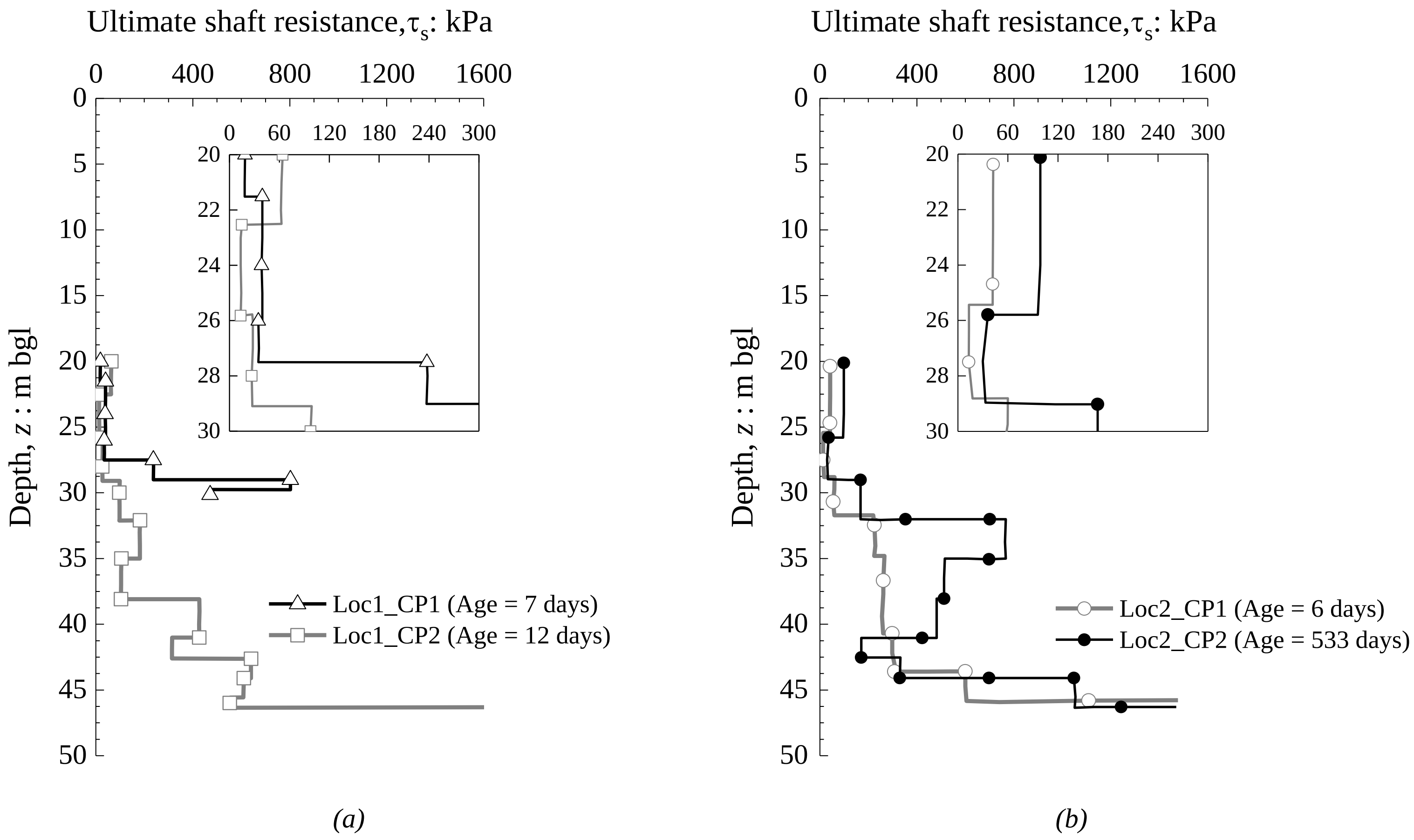

Figure 10 Distribution of shaft resistance from static tests (adapted from Kolk et al. 2005): (a) Location 1; (b) Location 2

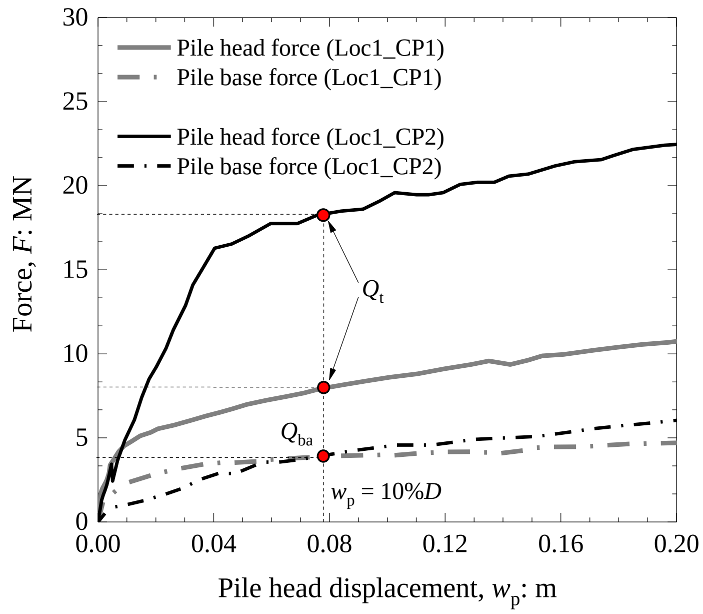

(a)

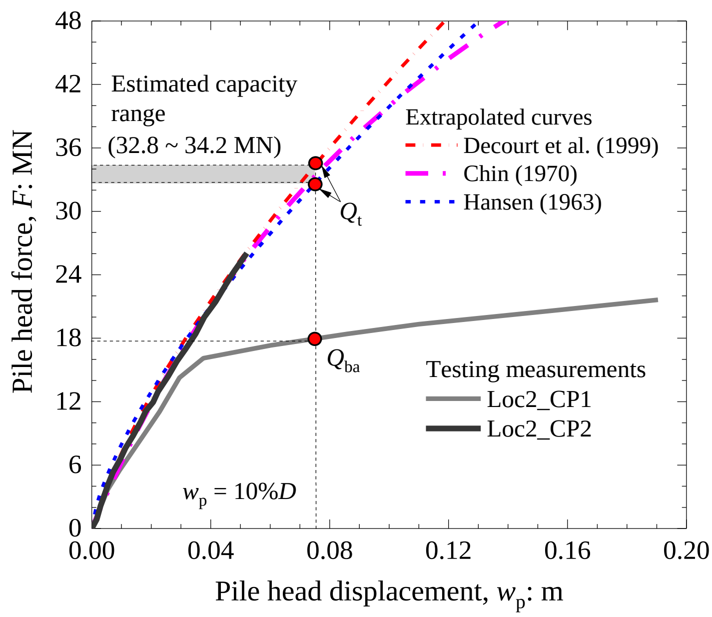

(b)

Figure 11 Force measured at pile head and toe versus pile head displacement, (a) Location 1; (b) Location 2

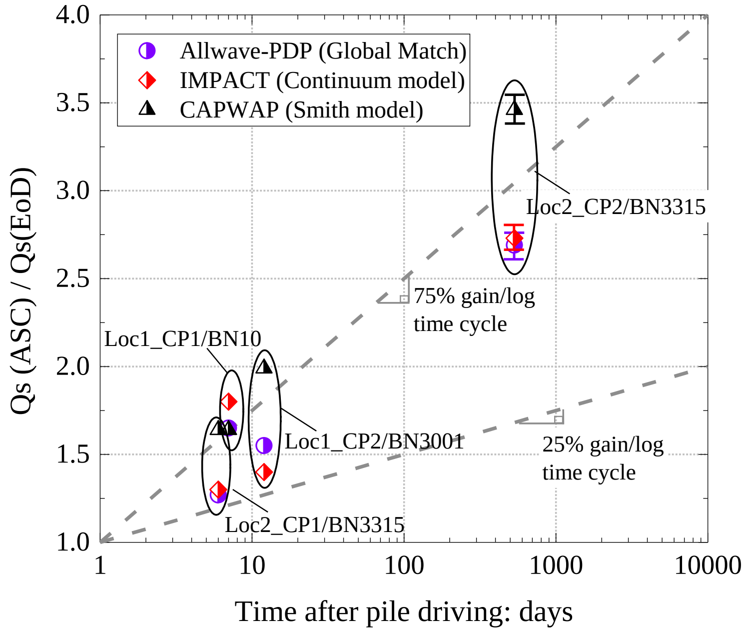

Figure 12 Qs(ASC)/Qs(EoD) versus ageing days after driving

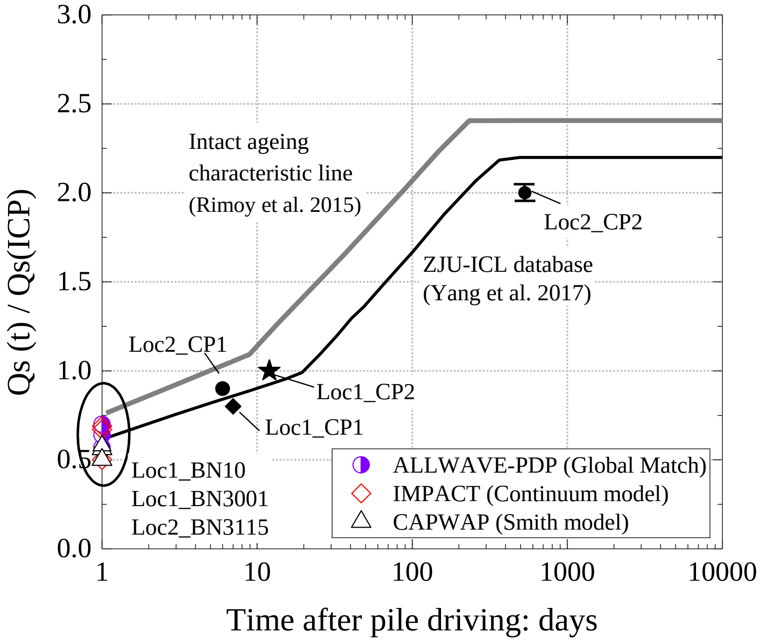

Figure 13 Qs(t)/ Qs(ICP) versus ageing days after driving

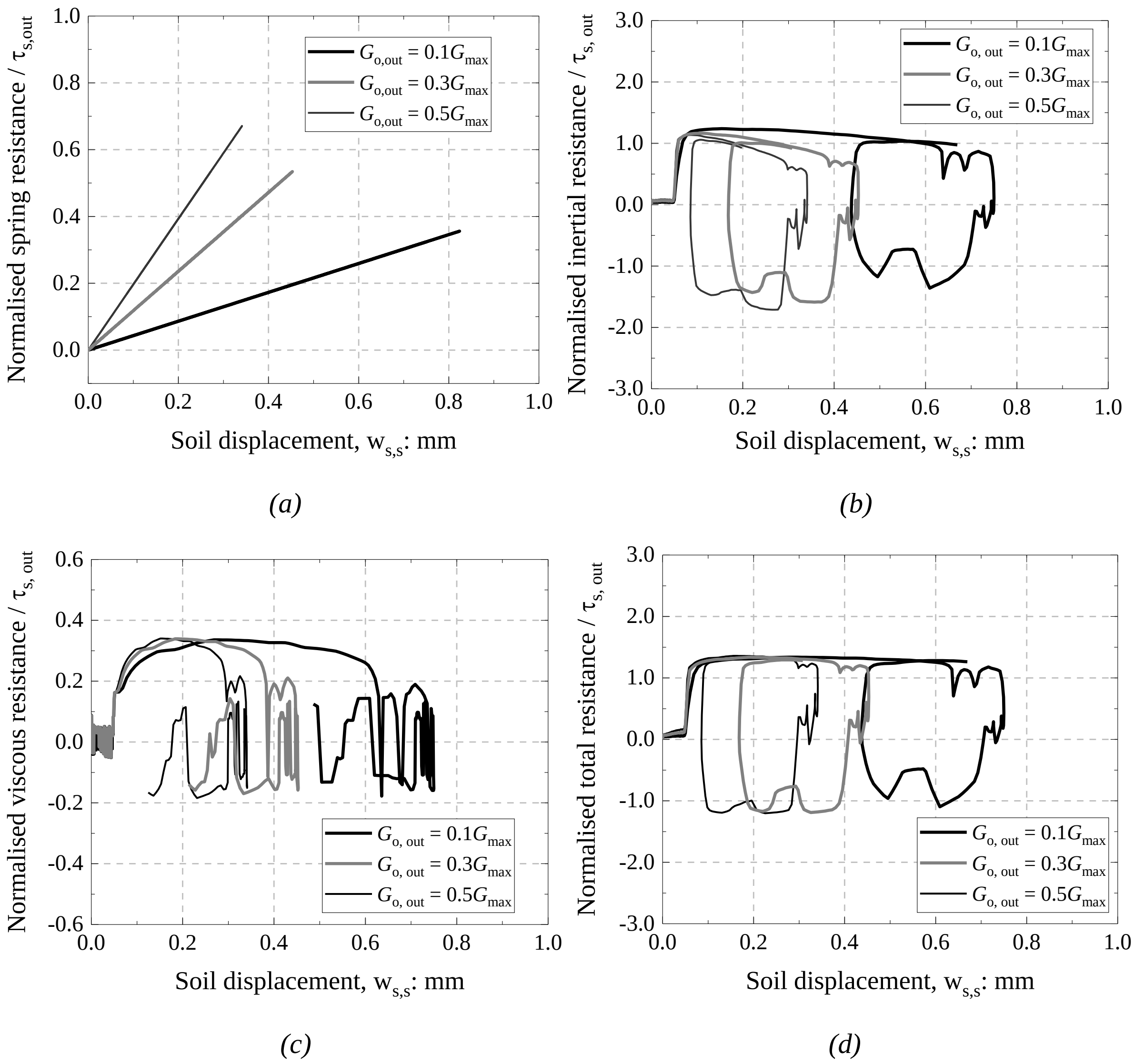

Figure A-1 Effect of operational shear modulus $G_{o,out}$ on a typical soil element outside pile wall: (a) spring, (b) radiation dashpot, (c) viscous dashpot, (d) total resistance

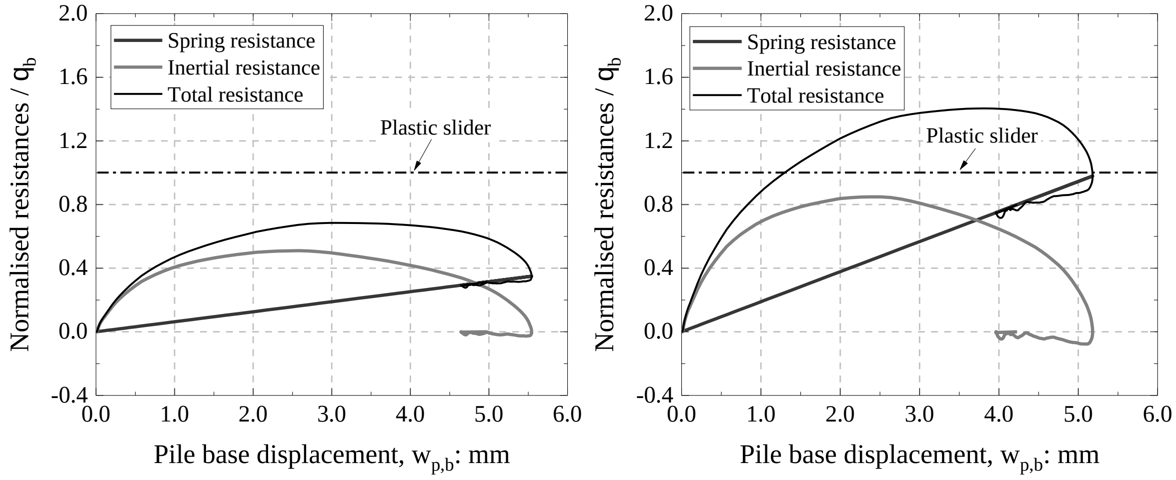

(a) *(b)*

Figure A-2 Effects of $G_{o,b}$ on the performance of a pile base element (a) $G_{o,b} = 0.2G_{max}$; (b) $G_{o,b} = 0.6G_{max}$

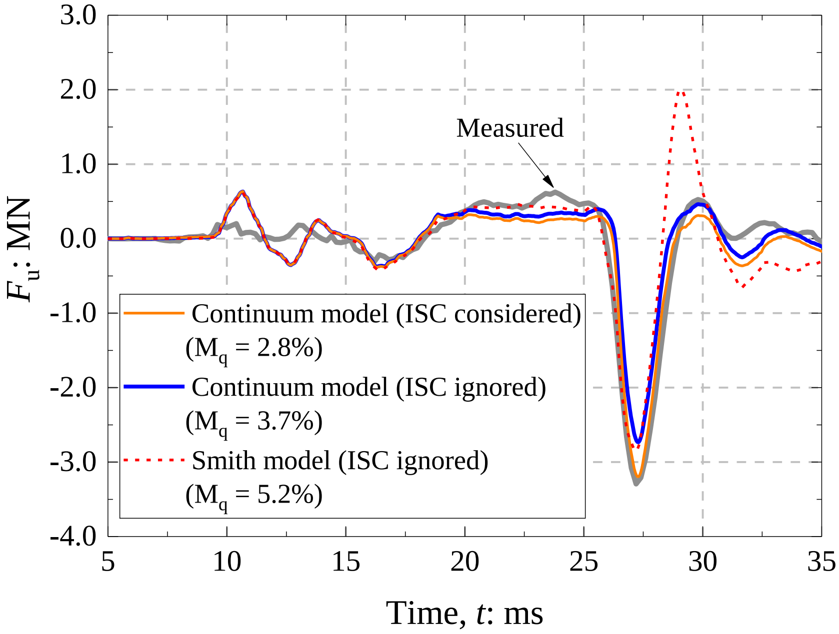

Figure A-3 Effect of modelling internal soil column explicitly on signal matching

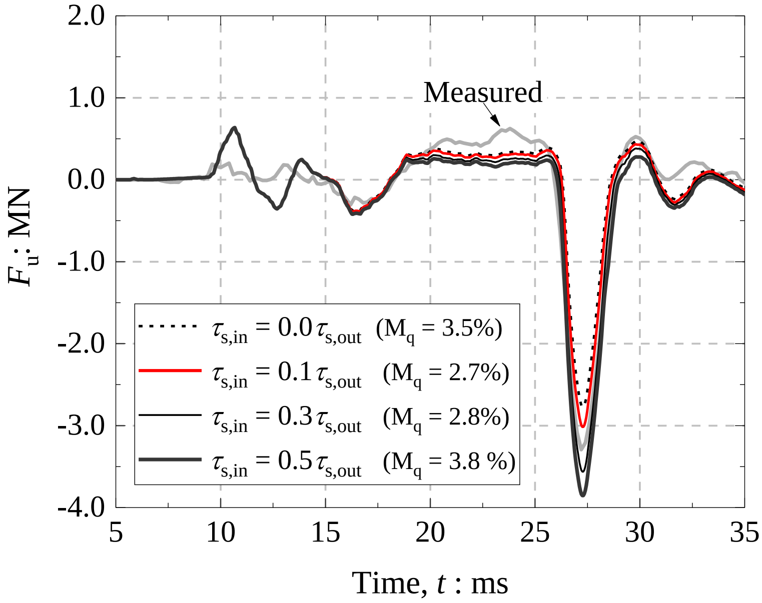

(a)

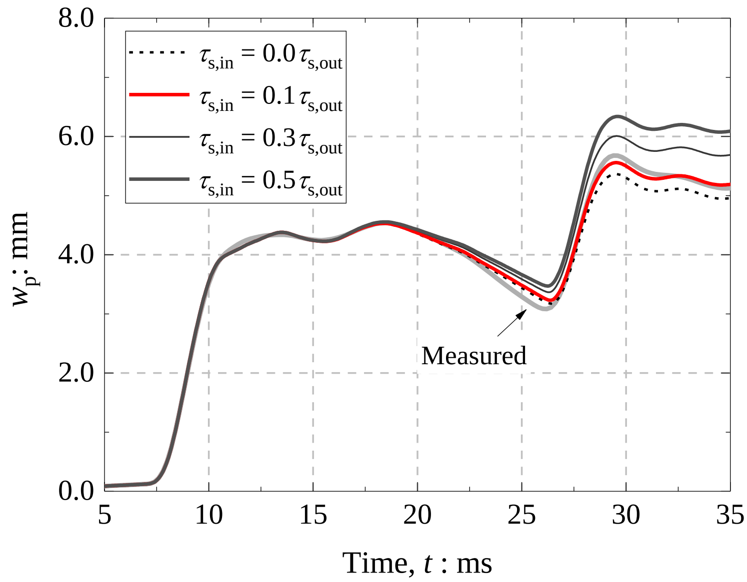

(b)

Figure A-4 Effects of ratios of internal to external resistances (a) upward travelling wave; (b) pile head displacement

NOTATION

A	Steel cross section area
D	Pile outer diameter
D_i	Pile inner diameter
D_r	Relative density
E	Young's modulus
$F_{u,m}$	Measured upward travelling force
$F_{u,c}$	Calculated upward travelling force
F_{max}	Maximum force measured at pile head
G	Shear modulus
G_{max}	Maximum shear modulus
$G_{o,out}$	Operational shear modulus for soils outside pile wall
$G_{o,in}$	Operational shear modulus for soils inside pile wall
$G_{o,b}$	Operational shear modulus for soils beneath pile base
h	Relative depth to pile tip
J_s	Smith damping constant for pile shaft
J_b	Smith damping constant for pile base
I_c	Soil behaviour type index
L	Pile length
M_q	Matching quality
n_{sample}	Number of the sample time increments in a given time period
q_c	Cone tip resistance
$q_{b,a}$	Limiting end-bearing pressure beneath pile's annular base
Q_s	Pile shaft capacity
$Q_{p,s}$	Quake for pile shaft node
$Q_{p,b}$	Quake for pile base node
Q_{ba}	Pile annual base capacity
Q_t	Pile total capacity
R^*	Equivalent radius for open-ended piles
R_{max}	Maximum surface roughness
t	Time
t_w	Pile wall thickness
$T_{s,in}$	Internal shear force per unit length
V	Velocity at pile head
v	Poisson's ratio
$v_{s,s}$	Local soil velocity beneath pile base
$v_{p,s}$	Local pile shaft velocity
$v_{p,b}$	Local pile base velocity
v_{ref}	Reference velocity
W	Dry weight per unit length
w_p	Pile head displacement

$w_{p,s}$	Local pile shaft displacement
$w_{p,b}$	Local pile base displacement
$w_{s,s}$	Local soil displacement along pile shaft
$w_{s,b}$	Local soil displacement beneath pile base
Z	Pile impedance
α	Viscosity parameter in Continuum model
β	Viscosity parameter in Continuum model
σ_e	Yield strength of steel pile
σ_v'	Vertical overburden effective stress
σ_{ri}'	Local radial effective stress
δ'	Interface friction angles
ρ	Mass density
τ	Total shaft resistance during driving (static + dynamic)
τ_{lim}	Velocity-dependent limiting resistance at pile-soil interface
τ_s	Limiting static shaft resistance (external + internal)
$\tau_{s,in}$	Limiting resistance on pile internal shaft
$\tau_{s,out}$	Limiting resistance on pile outer shaft
ASC	Axial static compression
bgl	Below ground level
BH	Borehole tests
BoR	Beginning of restrike
CPT	Cone penetration tests
CRP	Constant rate of penetration
EoD	End of driving
EURIPIDES	European Initiative on Piles in Dense Sands
IFR	Incremental filling ratios
ISC	Internal soil column
JIP	Joint industry project
PAGE	Pile ageing in sands
SRD	Static resistance to driving